Acta Pharmaceutica Sinica B 2025;15(8):4174–4192

Chinese Pharmaceutical Association
Institute of Materia Medica, Chinese Academy of Medical Sciences

Acta Pharmaceutica Sinica B

www.elsevier.com/locate/apsb
www.sciencedirect.com

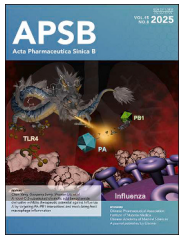

ORIGINAL ARTICLE

High-efficient discovering the potent anti-Notum agents from herbal medicines for combating glucocorticoid-induced osteoporosis

Yuqing Song[a,†], Feng Zhang[a,b,†], Jia Guo[c,†], Yufan Fan[a], Hairong Zeng[a], Mengru Sun[a], Jun Qian[d], Shenglan Qi[a], Zihan Chen[a], Xudong Jin[e], Yunqing Song[a], Tian Tian[a], Zhi Qian[b], Yao Sun[d], Zhenhao Tian[a,f,*], Baoqing Yu[b], Guangbo Ge[a,*]

[a]*State Key Laboratory of Discovery and Utilization of Functional Components in Traditional Chinese Medicine, Shanghai Frontiers Science Center of TCM Chemical Biology, Institute of Interdisciplinary Integrative Medicine Research, Shanghai University of Traditional Chinese Medicine, Shanghai 201203, China*
[b]*Department of Orthopedics, the Seventh People's Hospital, Shanghai University of Traditional Chinese Medicine, Shanghai 200137, China*
[c]*Shi's Center of Orthopedics and Traumatology, Shuguang Hospital Affiliated to Shanghai University of Traditional Chinese Medicine, Shanghai 201203, China*
[d]*Engineering Research Center of Tooth Restoration and Regeneration & Tongji Research Institute of Stomatology & Department of Oral Implantology, Stomatological Hospital and Dental School, Tongji University, Shanghai 201203, China*
[e]*University of Oxford, Oxford OX3 7BN, UK*
[f]*School of Life Sciences, Northwestern Polytechnical University, Xi'an 710072, China*

Received 4 January 2025; received in revised form 28 April 2025; accepted 5 May 2025

KEY WORDS

Notum;
NIR fluorogenic substrate;
High-throughput screening;

Abstract Notum, a negative feedback regulator of the Wnt signaling, has emerged as a promising target for treating glucocorticoid-induced osteoporosis (GIOP). This study showcases an efficient strategy for discovering the anti-Notum constituents from herbal medicines (HMs) as novel anti-GIOP agents. Firstly, a rapid-responding near-infrared fluorogenic substrate for Notum was rationally engineered for high-throughput identifying the anti-Notum HMs. The results showed that Bu-Gu-Zhi (BGZ), a known

*Corresponding authors.
E-mail addresses: zhhtian@nwpu.edu.cn (Zhenhao Tian), geguangbo@shutcm.edu.cn (Guangbo Ge).
[†]These authors made equal contributions to this work.
Peer review under the responsibility of Chinese Pharmaceutical Association and Institute of Materia Medica, Chinese Academy of Medical Sciences.

https://doi.org/10.1016/j.apsb.2025.06.004

Glucocorticoid-induced osteoporosis (GIOP);
A high-efficient platform;
5-Methoxypsoralen;
Wnt signaling;
Osteoblast differentiation

anti-osteoporosis herb, potently inhibited Notum in a competitive-inhibition manner. To uncover the key anti-Notum constituents in BGZ, an efficient strategy was adapted *via* integrating biochemical, phytochemical, computational, and pharmacological assays. Among all identified BGZ constituents, three furanocoumarins were validated as strong Notum inhibitors, while 5-methoxypsoralen (5-MP) showed the most potent anti-Notum activity and favorable safety profiles. Mechanistically, 5-MP acted as a competitive inhibitor of Notum *via* creating strong hydrophobic interactions with Trp128 and Phe268 in the catalytic cavity of Notum. Cellular assays showed that 5-MP remarkably promoted osteoblast differentiation and activated Wnt signaling in dexamethasone (DXMS)-challenged MC3T3-E1 osteoblasts. In dexamethasone-induced osteoporotic mice, 5-MP strongly elevated bone mineral density (BMD) and improved cancellous and cortical bone thickness. Collectively, this study constructs a high-efficient platform for discovering key anti-Notum constituents from HMs, while 5-MP emerges as a promising anti-GIOP agent.

1. Introduction

Osteoporosis (OP), a systemic bone metabolic disease, has become a significant global health concern due to the aging populations worldwide[1,2]. OP is characterized by decreased bone mineralization and reduced bone mass, leading to an increased risk of fractures[3]. As a prevailing skeletal disease of the elderly, nearly 200 million osteoporotic patients are diagnosed annually, while approximately 9.3 million osteoporotic fractures occur globally each year[4,5]. OP can be subdivided into two main categories, primary and secondary osteoporosis. Primary OP is an age-related disorder that encompasses postmenopausal osteoporosis and senile osteoporosis. By contrast, secondary OP has a clearly definable etiologic mechanism (such as malabsorption and medications), while glucocorticoid-induced osteoporosis (GIOP) is the most common form of secondary OP[6]. Growing evidence indicates a strong link between glucocorticoid (GC) therapy and osteoporosis, making it the leading cause of drug-induced osteoporosis. Over 30% of patients on long-term GC treatment suffer osteoporotic fractures[7]. Dexamethasone (DXMS), one of the most commonly used GCs, can cause severe complications, including femoral head necrosis, osteoporosis, and other bone-related disorders[8]. The principal etiological factor of GC-related bone disorders is believed to be GC-induced apoptosis of osteoblasts and osteocytes. Although some medications (such as bisphosphonates, anti-RANKL antibodies, and selective estrogen receptor modulators like teriparatide) have been recommended to manage GIOP, these agents may cause non-negligible toxicities or side effects[9]. Thus, there is an urgent need to develop more efficacious therapeutic agents with favorable safety profiles for combating GIOP.

As a highly conserved signaling in biological evolution, the Wnt signaling plays a crucial role in regulating stem cell renewal, cell proliferation, and differentiation[10,11]. The Wnt signaling is also essential for maintaining bone density and stimulating osteoblast activity[12]. However, long-term exposure to GCs significantly suppresses the Wnt signaling and downregulates osteogenic differentiation-related genes in both osteoblasts and osteoclasts[13]. It is well-known that Wnt proteins are notoriously difficult to target pharmacologically[14], developing direct Wnt-based therapies is a huge challenge. To overcome this limitation, researchers have explored alternative druggable regulators of the Wnt signaling, such as Notum[15], Dickkopf (DKK) proteins[16], sclerostin/SOST family proteins[17], secreted FZD-related proteins (sFRPs)[18], and Wnt inhibitory proteins (WIF proteins)[10,19]. Among all reported druggable regulators of Wnt signaling, Notum, a palmitoyl protein carboxylase, has attracted significant attention due to its systemic multi-organ distribution and its crucial role in blocking the Wnt signaling[20]. As an important α/β-serine hydrolase, Notum negatively regulates Wnt signaling by cleaving the palmitoleic acid moiety from Wnt proteins, thereby blocking the binding of Wnt proteins to frizzled receptor[21]. It has been reported that GCs (such as DXMS) could upregulate Notum in osteoblasts, leading to reduced cortical bone mass and triggering osteoporosis[22]. In contrast, pharmacological inhibition or genetic blockade of Notum could restore trabecular bone structure and enhance cortical bone thickness and strength, making Notum a promising therapeutic target for combating GIOP[23-25]. However, the potent Notum inhibitors with optimal druglike properties and favorable safety profiles are rarely reported, highlighting the urgent need to develop more efficacious Notum inhibitors through interdisciplinary approaches.

Herbal medicines (HMs) are often used for GIOP management in Asian countries[26], while parts of them have demonstrated clinically significant improvements in bone density and therapeutic benefits for GIOP patients[27,28]. However, the active anti-GIOP components in HMs and related anti-GIOP mechanisms remain largely unclear, primarily due to the absence of robust and efficient methods for identifying the key anti-GIOP constituents from crude herbal extracts. Structurally, Notum is a monomeric serine hydrolase containing a mobile cap structural domain and an α/β hydrolase fold domain critical for its hydrolytic function[21,29]. Notably, Notum possesses a single ligand-binding pocket (namely its catalytic pocket), making it an attractive target for structure-based drug discovery. To the best of our knowledge, all reported naturally occurring Notum inhibitors are non-covalent agents[29-36], functionally through competitive inhibition by directly occupying the catalytic pocket. More recently, several fluorescence-based biochemical assays were constructed[37-39] for rapidly discovering Notum inhibitors. However, existing fluorogenic substrates for Notum are constrained by their short-wavelength blue emission (<580 nm)[37,38,40], generating spectral interference when directly screening herbal extracts or the phytochemicals (such as coumarins or flavanols) emitting with fluorescence signals. In contrast, near-infrared fluorescent probes (NIRFPs) offer distinct advantages, including minimal background interference, superior spatiotemporal resolution, and enhanced tissue penetration[41,42].

Recent advances have enabled the successful application of NIRFPs in enzyme modulator screening, disease diagnostics, and organ function assessment[43,44], which encouraged us to develop more practical NIRFPs for highly efficient screening and characterization of herbal medicines (HMs) with potent anti-Notum effects.

This study aimed to construct a practical and efficient platform for discovering the naturally occurring potent Notum inhibitors from HMs to combat GIOP. Firstly, a novel, rapid-responding near-infrared fluorogenic substrate for Notum was developed to construct a practical fluorescence-based high-throughput screening assay, which was subsequently used to assess the anti-Notum potentials of the commonly used HMs. Following screening of more than one hundred herbal extracts, Bu-Gu-Zhi (BGZ), one of the most frequently used anti-osteoporosis herbs, was found with potent and competitive inhibition against Notum. These findings encouraged us to further uncover the key anti-Notum constituents in BGZ and to decipher their anti-osteoporosis effects and underlying molecular mechanisms. To achieve these goals, a highly efficient platform that integrates biochemical, phytochemical, computational, cellular, and *in vivo* assays, was constructed (as depicted in Scheme 1). With the help of this platform, three furanocoumarins, including 5-methoxypsoralen (5-MP), psoralen, and isopsoralen, were identified as strong Notum inhibitors (IC_{50} < 110 nmol/L), while 5-MP was the most potent one (IC_{50} = 18.73 nmol/L). Further investigations showed that psoralen and isopsoralen could cause significant organ injuries, while 5-MP showed a favorable safety profiles in mice. These findings prompted us to comprehensively investigate the *in vitro* and *in vivo* anti-osteoporosis effects of 5-MP, as well as its regulatory effects on Wnt/β-catenin signaling in osteoblasts.

2. Materials and methods

2.1. Chemicals and instruments

Citric acid and K_2HPO_4 were purchased from Sigma−Aldrich (USA). 8-Octanoyloxypyrene-1,3,6-trisulfonic acid trisodium salt (OPTS) was purchased from Sigma−Aldrich (USA). ABC99

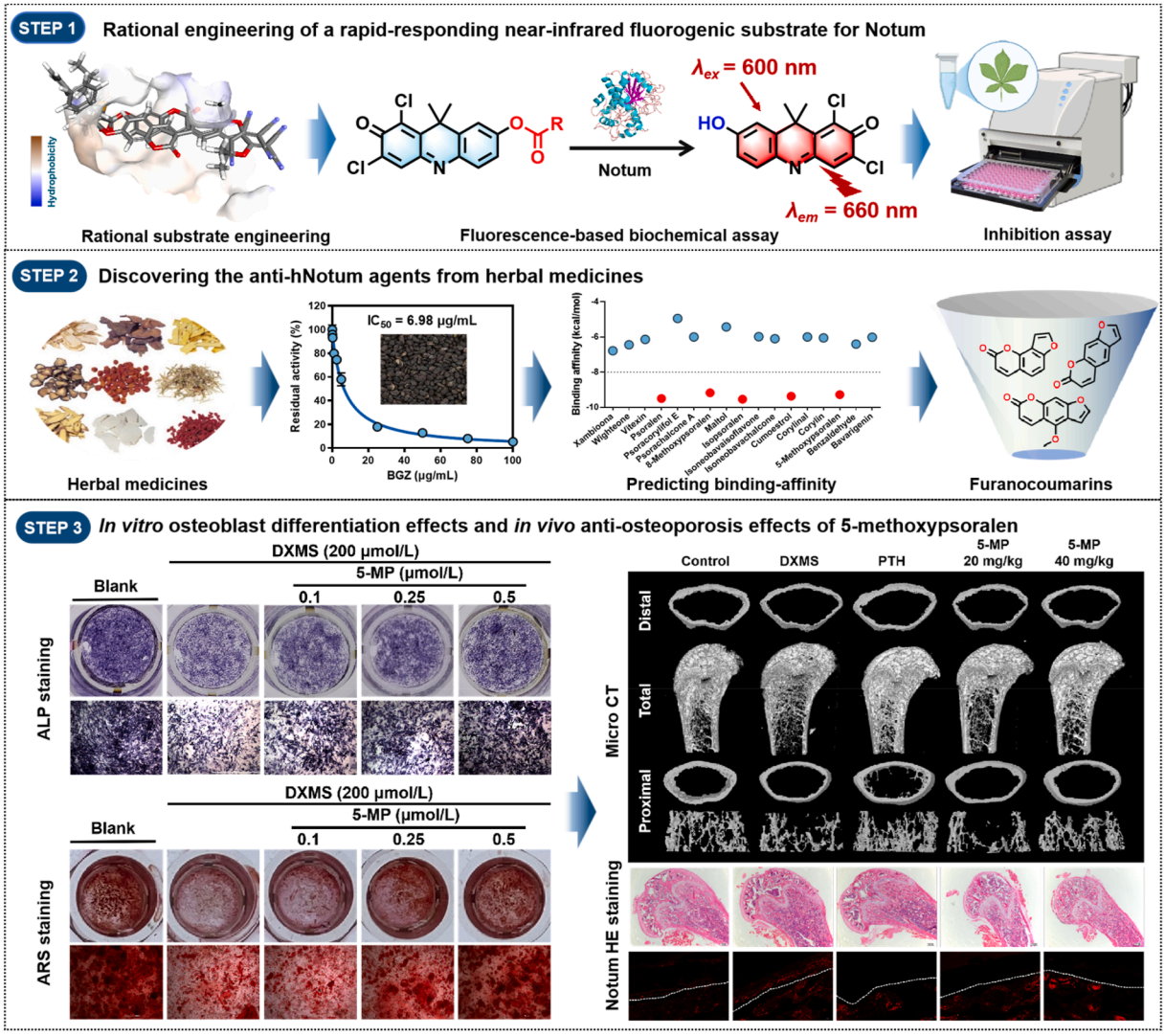

Scheme 1 The methodological framework for uncovering the anti-Notum constituents from herbal medicines and investigating their anti-osteoporotic effects. (1) Rational engineering of a rapid-responding near-infrared fluorogenic substrate for Notum. (2) Discovering the anti-hNotum agents from herbal medicines. (3) *In vitro* osteoblast differentiation effects and *in vivo* anti-osteoporosis effects of 5-methoxypsoralen.

was purchased from GlpBio Technology (USA). 5-Methoxypsoralen was provided by Shanghai BiDe Pharmaceutical Technology Co., Ltd. (China), mass spectrometry and NMR results for 5-MP are shown in Supporting Information Figs. S1−S3. Isopsoralen and psoralen were provided by Chengdu Pufei De Biotech Co., Ltd. (China). HPLC-grade optima® acetonitrile (ACN) was purchased from Fisher Scientific (USA). HPLC-grade formic acid (FA, 98%) was obtained from Aladdin (China). Fetal bovine serum (FBS), penicillin−streptomycin (10,000 U/mL), and cell culture medium (DMEM) were acquired from Gibco (Thermo Fisher Scientific, USA). Culture-treated plates were purchased from Corning (China). Cell Counting Kit-8 was purchased from Shanghai Yeasen Biotechnologies Co., Ltd. (China). Notum was expressed and purified for subsequent biochemical analysis[38]. The herbal extracts used in this study were provided by Shanghai Standard Technology Co., Ltd. (Shanghai, China). The ultrapure water used in the experiment was produced by the Milli-Q ultrapure water system.

2.2. Molecular docking simulations

Six crystal structures of Notum (PDB IDs: 6R8R, 6TUZ, 6YSK, 7BLS, 7BNB, and 8BTH) were downloaded from the Protein Data Bank (http://www.rcsb.org/). PDBQT files were prepared for the six receptor models by removing water molecules and excess heteroatoms, adding hydrogens, merging non-polar hydrogens, and adding Kollman charges according to standard protocols. All fluorogenic substrate candidates and constituents in HMs were drawn using ChemDraw 20.0, subsequently, energy minimization was performed using Chem3D 20.0. Molecular docking simulations were conducted by AutoDock Vina software. The distance between the carbonyl carbon of fluorogenic and the catalytic residue (Ser232) of Notum was measured using Pymol. Visualization was conducted using the Pymol and Discovery Studio software[40,41].

2.3. Hydrolytic rates of DDAO esters in notum

The incubation system (200 μL) contained Notum (0.1 μg/mL), CPB (0.1 mol/L, pH = 7.4), and **DDAO** ester. After pre-incubating at 37 °C for 1 min, the reactions were initiated by adding **DDAO** ester. Then, all samples were incubated in a microplate reader ($\lambda_{ex}/\lambda_{em}$ = 600/660 nm, SpectraMax® iD3, Molecular Devices, Austria) for 20 min at 37 °C and detected every 2 min. The hydrolytic activity of Notum was calculated using the quantitative calibration curve of the **DDAO** (0.001−10 μmol/L) (Supporting Information Scheme S1).

2.4. Notum inhibition assays

The anti-Notum effects were tested according to a previously reported high-throughput screening assay[42]. Briefly, a total of 200 μL incubation system comprising Notum, CPB (0.1 mol/L, pH = 7.4), and each tested inhibitor (1 μL), were pre-incubated at 37 °C for 1 or 21 min. Upon addition of the substrates OPTS/**DO**, all samples were incubated in a microplate reader ($\lambda_{ex}/\lambda_{em}$ = 403/510 nm for OPTS, $\lambda_{ex}/\lambda_{em}$ = 600/660 nm for **DO**, SpectraMax® iD3, Molecular Devices, Austria) for 20 min at 37 °C and detected every 2 min. The residual activity (%) of Notum was calculated by using the fluorescence intensity in the presence of inhibitors to the control (DMSO only).

2.5. Homology modeling of notum and its mutants

The protein sequence of homo sapiens Notum was obtained from the Uniprot database using the accession number Q6P988. The crystal structure of human Notum, with the PDB code 7BLS and a high resolution of 1.19 Å, was chosen as the primary template. After that, the sequences of two Notum mutants (Trp128Gly and Phe268Gly) were generated. Homology modeling was performed by aligning the target protein sequence with the known template using molecular operating environment (MOE) sequence alignment tools. Transfer coordinates from the template to the target in MOE when the residue identity is conserved. Collect backbone fragments from a high-resolution database and assemble alternative side chains from a rotamer library for non-identical residues. Construct multiple models based on loop and side-chain placements scored by a contact energy function. Refine the final model through energy minimization, selecting either a minimized Cartesian average structure or the best intermediate model.

2.6. Cell culture of MC3T3-E1 cells

The MC3T3-E1 cell line was purchased from the cell bank, Chinese Academy of Science (Shanghai, China). The cells were cultured in DMEM media supplemented with 10% FBS and 1% penicillin−streptomycin solution in a humidified culture chamber at 37 °C with 95% air and 5% CO_2.

2.6.1. Alkaline phosphatase (ALP) staining and alizarin red S (ARS) staining

MC3T3-E1 cells were seeded in 96-well plates at a density of 2×10^3 cells/well and cultured for 24 h. The medium was replaced with an inducible medium, and the cells were cultured with the simultaneous addition of DXMS and the target compound (5-methoxypsoralen/psoralen/isopsoralen) for seven days, and the medium was replaced every two days. Subsequently, the cells were fixed in 4% paraformaldehyde at room temperature for 15 min, then washed 2 to 3 times with PBS, and stained with the BCIP/NBT alkaline phosphatase staining kit. The cell staining images were performed by Cytation 5 (BIOTEK, USA). Next, to test the promoting effects of 5-methoxypsoralen on osteogenic differentiation, a series of concentrations of 5-methoxypsoralen were added in DXMS-challenged (200 μmol/L) MC3T3-E1 cells. The cells were cultured with DXMS and 5-methoxypsoralen for 21 days, while the medium was replaced every two days. After then, the MC3T3-E1 cells were fixed with 4% paraformaldehyde for 15 min, then washed 2 to 3 times with PBS, followed by staining with 0.2% ARS solution for 30 min. Following PBS rinsing, the cell staining images were performed by Cytation 5 (BIOTEK, USA).

2.6.2. Quantitative real-time PCR (qPCR)

MC3T3-E1 cells were cultured for 7 days, the cells were washed three times using pre-cooled PBS for total RNA analysis. RNA was extracted using MolPure Cell/Tissue Total RNA Kit (Yeasen, China) and determined by Nanodrop One (Thermo, USA). Following the instructions provided by the manufacturer, cDNA was synthesized using the Evo M-MLV RT Reverse Transcription Kit II (AG11711, Accurate Biotechnology). qPCR was performed using SYBR Green Pro Taq HS premixed qPCR kit (AG11701, Accurate Biotechnology) in an RT fluorescence quantitative PCR system (QuantStudio 6 Flex, Thermo Scientific, USA). The

relative gene expression was calculated using GAPDH as an internal reference. The primer sequences are presented in Supporting Information Table S1.

2.6.3. Western blotting (WB)

The cells were cultivated in 6-well plates for 24 h and subsequently treated with DXMS or 5-methoxypsoralen for seven days. The medium was replaced every two days. On the 7th day, the cells were initially rinsed twice with PBS and lysed using RIPA buffer, supplemented with 1% phosphatase inhibitor and 1% protease inhibitor. The protein concentration of lysates was determined by utilizing the Nanodrop One (Thermo Scientific, USA) spectrophotometer. The proteins were separated using 7.5% sodium dodecyl sulfate-polyacrylamide gel electrophoresis, followed by membrane transfer, sealing, and overnight incubation of the primary antibody at 4 °C. Subsequently, the PVDF membrane was incubated with secondary antibody (titer 1:10,000) for 1 h at room temperature. Protein bands were visualized using Enhanced Chemiluminescence. The relative expression level of the proteins was calculated by using GAPDH as an internal reference. Antibodies against active β-catenin (CST, USA), β-catenin (Abways, China), OPN (ABclonal, China), GSK3β (Proteintech, USA), Notum (Abcam, UK), RUNX2 (ABclonal, China) and GAPDH (CST, USA) were used at a dilution of 1:1000, 1:1000, 1:1000, 1:1000, 1:1000, 1:1000 and 1:10,000, respectively. The Image J analysis system was used to analyze chemiluminescent data.

2.7. Animals

SPF grade C57BL/6J mice were purchased from Shanghai SLAC Laboratory Animal Co., Ltd. and housed in the Experiment Animal Center of Shanghai University of Traditional Chinese Medicine. This study was approved by the Animal Ethics Committee of Shanghai University of Traditional Chinese Medicine (license No. PZSHUTCM2404280002). Mice were maintained under specific pathogen-free conditions and standard laboratory conditions. The environmental conditions were 25 ± 2 °C, 50 ± 10% humidity, free access to food and water, and 12 h/12 h light/dark cycles. All mice were subjected to adaptive feeding for 7 days before the experiment.

2.7.1. Toxicity test of 5-methoxypsoralen, isopsoralen, psoralen in mice

A total of 32 C57BL/6J mice (16 males and 16 females) with an average weight of 18−20 g were randomly assigned into four groups (4 males and 4 females). 5-Methoxypsoralen/isopsoralen/psoralen was dissolved in 0.5% CMC-Na, and mice were orally administered 5-methoxypsoralen/isopsoralen/psoralen (200 mg/kg)/0.5% CMC-Na continuously for 14 days. The mice were weighed every two days, and their status was observed. After 14 days, blood and tissues from all mice were obtained for safety assessment. Aspartate aminotransferase (AST), aminotransferase (ALT), ALP, albumin (ALB), blood urea nitrogen (UREA), creatinine (CREA), creatine kinase (CK), total cholesterol (TC), triglycerides (TG), and total protein (TP) levels of serum were tested by utilizing a fully automated serum biochemistry analysis (Thermo, USA). Hematoxylin and eosin (H&E) stains of the mice organ were provided by Ningbo Yangming Medical Laboratory Co., Ltd.

2.7.2. Tissue distribution of 5-methoxypsoralen

A total of twenty C57BL/6J male mice (aged 6 weeks, 18−20 g) were randomly assigned into four groups (control group, after administration 1 h group, 2 h group, and 3 h group). 5-Methoxypsoralen (40 mg/kg) was dissolved in 0.5% CMC-Na and administered by gavage. Then, the mice were anesthetized after being administered 0, 1, 2 and 3 h, respectively. The blood and organs (including the liver, heart, spleen, lung, kidney, brain, muscle, and femur) were rapidly removed for subsequent analysis. After that, each tissue sample was weighed after the surface of the tissue was aspirated. The tissues were then transferred to EP tubes and dissected with scissors. PBS (pH 7.4) and magnetic beads were added to the EP tubes, and the tissues were homogenized using a tissue grinder (Thermo, USA). 40 μL of tissue supernatant was diluted with 160 μL of LC-grade acetonitrile (with internal standard) and vortexed for 1 min. The samples were centrifuged at 20,000×g at 4 °C for 30 min. The concentration of 5-methoxypsoralen was then determined by LC−MS/MS analysis, with the parameters of mass spectrometry analysis shown in Supporting Information Table S2.

2.7.3. In vivo anti-osteoporosis tests

Thirty C57BL/6J male mice (aged 6 weeks) were randomly assigned to five groups. All mice were subjected to adaptive feeding for 7 days before the experiment. Osteoporosis model mice were constructed by receiving dexamethasone (DXMS, intraperitoneal injection) at a dose of 2.5 mg/kg for five weeks (five times a week). The 5-methoxypsoralen-treated group of mice was orally administered at low (20 mg/kg) and high (40 mg/kg) doses daily. The parathyroid hormone 1−34 ($PTH_{1\text{-}34}$, HY-P1252, MCE, USA) was used as a positive drug for treating osteoporosis, while this agent was administered *via* intraperitoneal injection (100 μg/kg/day). Following treatment for five weeks, serum, femurs, and tibias of each mouse in different groups were collected for subsequent analysis.

2.8. Detection of serum biochemical indicators

Serum samples were collected and the levels of bone metabolism indices, including alkaline phosphatase (ALP), osteocalcin/beta-glucuronidase (OT/BGT), osteoprotegerin (OPG), and collagen type I alpha 1 chain (Col-1A1), were measured using commercial enzyme-linked immunosorbent assay (ELISA) kits (ABclonal Biotech Co., Ltd., China) according to the manufacturer's instructions for quantitative assays.

2.9. Micro-CT assessments

All extracted mouse right femurs were fixed in a 4% paraformaldehyde solution. Subsequently, the specimens were scanned using a Skyscan1172 (Bruker, Germany) to visualize bone trabeculae and bone cortex. The scanning parameters were as follows: voltage 80 kVp, current 124 μA, section thickness 9.91 μm, and threshold range 65−225. Meanwhile, 100−200 layers of the distal femur growth plate were defined as the distal femur, and 300−400 layers were defined as the middle femur. The results were then analyzed accordingly using MicroView software.

2.10. H&E staining

Tissue slices were immersed in 10% EDTA solution and subjected to continuous decalcification using a multifunctional microwave processor. After decalcification, tissue slices were rinsed with PBS and H&E stained according to standard protocols (BBI, China). Paraffin-embedded samples were cut into 4 μm-thick slices, then

deparaffinized and rehydrated. Each slice was then stained with H&E for 10 and 2 min, respectively, then rinsed with distilled water and dehydrated.

2.11. Double labeling for assessing bone formation

Prior to specimen collection, 5 mg/kg calcein and 5 mg/kg dimethylphenol orange were injected intraperitoneally into mice on Days 14 and 1, respectively. The tibia sections were embedded in a photosensitive resin (EXAKT, Germany) and exposed to light for a 13.5-h period. The mineralized tissue was then sectioned and milled using the EXAKT system, with the resulting sections cut into 40 μm-thick slices[43,44].

2.12. Immunofluorescence of the mouse femur

Sections were deparaffinized with xylene and ethanol, and the antigen was recovered with Antigen Recovery Solution. Sections were then incubated with a blocking solution for 30 min. A 1:100 dilution of anti-Notum antibody (ab106448, Abcam, UK) was then applied and incubated at 4 °C overnight. The films were then incubated with secondary antibodies-488-conjugated goat anti-mouse IgG (H + L) (AS037, ABclonal, China) for 1 h at room temperature and then washed. Subsequently, the films were stained with fluorescent dyes and sealed with an anti-fluorescent quenching encapsulant (containing DAPI) (Servicebio, China) and sealing medium. The fluorescence signal was carried out using a fluorescence microscope.

2.13. Statistical analysis

All data are expressed as the mean ± standard deviation (SD). The K_m, $IC_{50,}$ and inhibition kinetics constant (K_i) values were determined *via* non-linear regression analysis using GraphPad Prism software. Nonparametric *t*-tests and one-way ANOVA were employed for group comparisons, with statistical significance set at $P < 0.05$. All statistical analyses were carried out using GraphPad Prism software (GraphPad Prism 8.0), and Origin (2025).

3. Result

3.1. Rational engineering of a near-infrared fluorogenic substrate for Notum

Previous studies have found that Notum preferentially hydrolyzes the substrates bearing a *n*-octanoate ester moiety[21], which can be used for designing the practical Notum-activatable fluorogenic substrate *via* introducing a *n*-octanoate ester moiety on fluorophores. Herein, ten near-infrared fluorophores (the emission wavelengths >580 nm) were collected, and their corresponding *n*-octanoate esters were designed and docked individually with six reported crystal structures of Notum one by one (PDB ID: 6R8R, 6TUZ, 6YSK, 7BLS, 7BNB, and 8BTH). As shown in Supporting Information Fig. S4, all designed fluorogenic substrate candidates showed favorable binding affinities towards Notum, but only **DDAO** *n*-octanoate (**DO**) showed high potential as a good substrate for Notum, owing to the distance between the carbonyl carbon of **DO** and the catalytic residue of Notum (Ser-232) was within 5 Å. By contrast, other fluorogenic substrate candidates showed oversized steric hindrance or excessively long dimensions, showing that the distances between the carbonyl carbon of substrates and catalytic residue Ser-232 of Notum exceeded 5 Å, indicating that these substrates were hardly hydrolyzed by Notum. Considering that Notum has a large hydrophobic active pocket that can accommodate carbon chain lengths of up to C16 (such as Wnt's palmitoleic acid ester), further structural modifications on **DDAO** were performed to synthesize more **DDAO** esters as fluorescent substrate candidates for Notum (DDAO 7-*n*-butyrate (**DB**), DDAO 7-*n*-hexanoate (**DH**), **DO**, DDAO 7-*n*-decanoate (**DDE**), DDAO 7-*n*-dodecanoate (**DDO**), DDAO 7-*n*-tetradecanoate (**DT**), DDAO 7-*n*-hexadecanoate (**DHE**), which were fully characterized by NMR and high-resolution mass spectrometry (Supporting Information Figs. S5−S25). Meanwhile, the hydrolytic rates of seven fluorescent substrate candidates in Notum were carefully evaluated, while **DDAO** 7-*n*-octanoate (**DO**) showed the fastest hydrolytic rate and the highest fluorescence intensity gain (Supporting Information Fig. S26). The anti-interference activity of **DO** was also investigated, and the results showed that the common metal ions and amino acids could not affect **DO** hydrolysis and **DDAO** quantification (Supporting Information Fig. S27). These findings suggest that **DO** is a rapid-responding near-infrared fluorescent substrate for Notum, encouraging us to further investigate the sensing properties of **DO**.

As shown in Fig. 1A−D, upon the addition of Notum, **DO** could be rapidly hydrolyzed to release a bright fluorescence product (**DDAO**), which emitted an NIR fluorescence signal around 660 nm. The fluorescence signal around 660 nm was significantly enhanced by 15.5-fold when **DO** was co-incubated with Notum for 20 min (Fig. 1E). The hydrolytic product **DDAO** exhibited stable fluorescent signals around 660 nm over a wide pH range (7.02−11.75) (Fig. 1F). Moreover, good linear relationships were observed between fluorescence intensity and Notum concentration (0−200 ng/mL), as well as reaction time (0−20 min) (Fig. 1G and H). As shown in Fig. 1I, Notum-catalyzed **DO** hydrolysis followed classical Fig. S6A—S6C) Michaelis−Menten kinetics, with K_m and V_{max} values of 0.19 μmol/L, and 1.13 μmol/min/mg Notum, respectively. These findings demonstrate that **DO** is a rapid-responding Notum substrate, showing both high binding affinity and rapid metabolic velocity. Meanwhile, ABC99 (a potent Notum inhibitor) could dose-dependently inhibit Notum-catalyzed **DO** hydrolysis, showing an IC_{50} value of 44.22 nmol/L (Fig. 1J). These results clearly demonstrate that **DO** is a rapid-responding near-infrared fluorescent substrate for Notum, making it a promising tool for constructing a fluorescence-based biochemical assay for the efficient discovery of Notum inhibitors.

3.2. BGZ shows the most potent anti-Notum effect

Next, a fluorescence-based high-throughput screening method was constructed using **DO** as a fluorescent substrate for screening and characterization of naturally occurring inhibitors of Notum from herbal medicines. The anti-Notum potential of 100 commonly clinically used herbal medicines was tested at a single dose (100 μg/mL, final concentration). As shown in Fig. 2A and Supporting Information Table S3, all tested herbal medicine extracts showed differential inhibitory effects against Notum-catalyzed **DO** hydrolysis. Interestingly, among all tested herbal extracts, BGZ, a commonly used anti-osteoporosis drug in clinical settings, showed the most potent anti-Notum effect, with a residual enzyme activity of only 1.66% at the dose of 100 μg/mL. Consequently, the inhibitory potency of BGZ against Notum was carefully studied. As shown in Fig. 2B, BGZ could dose-dependently inhibit

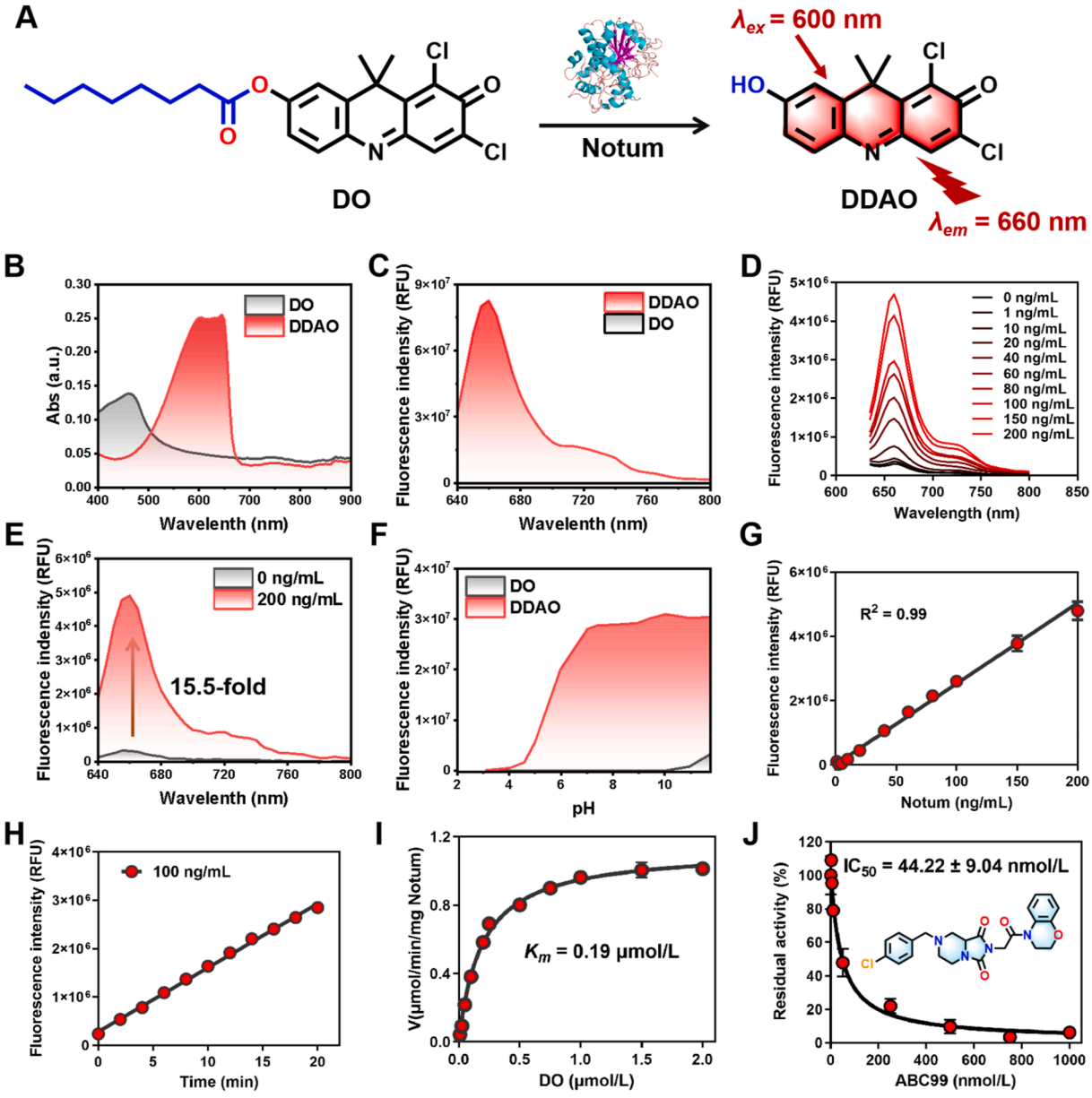

Figure 1 Rational engineering of a near-infrared fluorogenic substrate for Notum. (A) The sensing mechanism of **DO** towards Notum. (B) The absorption spectrum of **DO** and **DDAO**. (C) Emission spectrum of **DO** and **DDAO**. (D) Fluorescence response of **DO** towards increasing concentrations of Notum (ranging from 0 to 200 ng/mL) at 37 °C for 20 min. (E) The change in the emission spectrum of **DO** in the presence of Notum (200 ng/mL) at 37 °C for 20 min, λ_{ex} = 600 nm. (F) Effects of pH on the fluorescence intensities of **DO** and **DDAO**. The different pH values were adjusted by HCl and NaOH. λ_{ex} = 600 nm. (G) The linear relationship between the fluorescence intensity of **DDAO** and the concentrations of Notum (0−200 ng/mL). (H) The linear relationship between the fluorescence intensity of **DDAO** and the reaction time (0−20 min). (I) Michaelis−Menten plot of **DO** hydrolysis in Notum. (J) The dose−inhibition curve of ABC99 against Notum.

Notum-catalyzed **DO** hydrolysis (IC_{50} = 6.98 μg/mL). It was also found that the inhibitory effect of BGZ on Notum was not significantly enhanced after prolonging the pre-incubation time, suggesting that the inhibition of BGZ against Notum was reversible (Supporting Information Fig. S28A). Subsequently, inhibition kinetic assays further revealed that BGZ strongly inhibited Notum-catalyzed **DO** hydrolysis in a competitive inhibition manner, with a K_i value of 4.28 μg/mL (Fig. 2C and Fig. S28B). These findings clearly demonstrate that BGZ exhibits potent and competitive inhibition on Notum, prompting us to further uncover the key anti-Notum constituents in BGZ *via* integrating multiple technologies.

3.3. Global phytochemical analysis of BGZ by UHPLC−Q-Orbitrap HRMS

Next, a global phytochemical analysis of BGZ was performed by UHPLC−Q-Orbitrap HRMS, aiming to comprehensively identify the major constituents in BGZ. As shown in Fig. 3 and Supporting Information Table S4, a total of 83 constituents in BGZ were

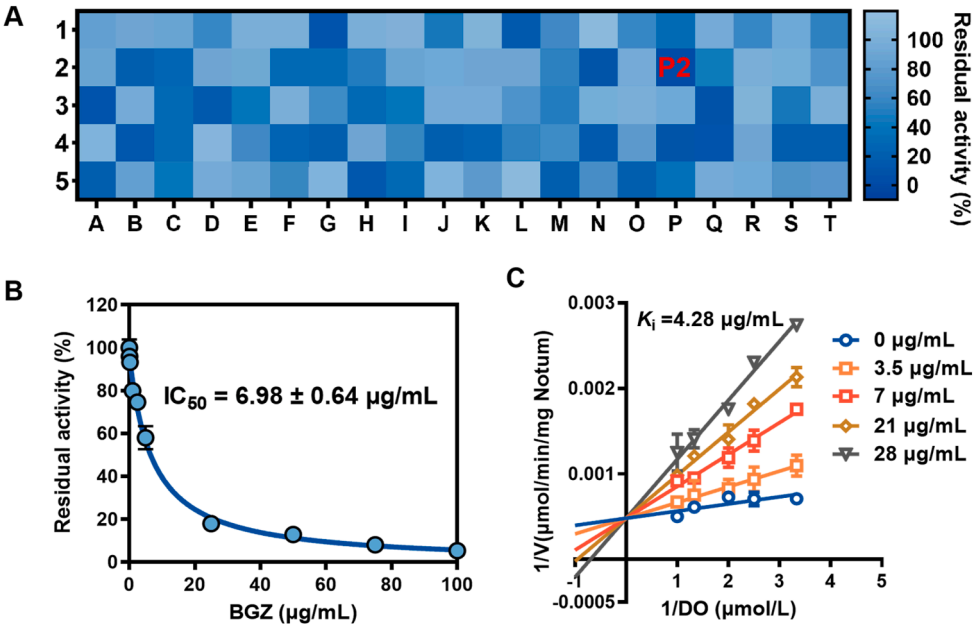

Figure 2 BGZ shows the most potent anti-Notum effect. (A) The inhibitory potentials of 100 herbal medicines (100 μg/mL, final concentration) against Notum-catalyzed **DO** hydrolysis. P2 refers to the extract of BGZ. (B) Dose−response curves of BGZ extract against Notum, with the IC_{50} values of 6.98 μg/mL. (C) Inhibition kinetics of BGZ extract toward Notum. All data are expressed as mean ± SD (n = 3).

identified in both positive and negative ion modes[45-47]. These constituents could be tentatively identified as coumarins, flavonoids, flavanones, chalcones, polyphenols, and other chemicals, by comparing the MS/MS spectra with the commercially available standards or previously reported phytochemicals or the natural compound databases. The retention times, pseudo-molecular ions, and molecular formula of all identified constituents in BGZ are listed in Table S4.

3.4. *Discovering the key anti-Notum constituents in BGZ*

To efficiently uncover the key anti-Notum constituents that inhibited Notum in BGZ, docking-based virtual screening was used to discover the natural compounds in BGZ with high-binding affinities towards Notum. As shown in Fig. 4A, 83 constituents in BGZ exhibited differential predicted binding energy within the catalytic pocket of Notum, with five constituents

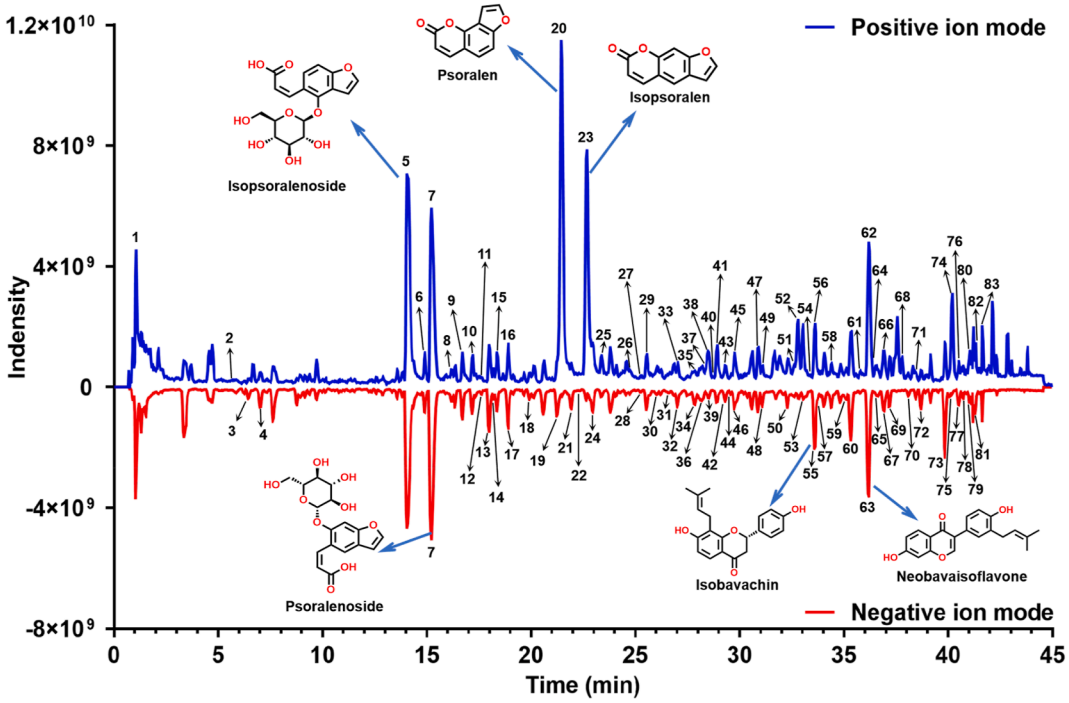

Figure 3 Global phytochemical analysis of BGZ by UHPLC−Q-Orbitrap HRMS in both positive and negative ion modes.

(including isopsoralen, psoralen, coumestrol, 5-methoxypsoralen, and 8-methoxypsoralen) showing high binding affinities (the predicted binding energy < -9.0 kcal/mol) towards Notum (Fig. 4B−F and Table 1). After then, the anti-Notum effects of these five constituents in BGZ (isopsoralen, psoralen, coumestrol, 5-methoxypsoralen, and 8-methoxypsoralen) were tested. As shown in Fig. S28C, 5-methoxypsoralen, isopsoralen, psoralen, 8-methoxypsoralen, and coumestrol dose-dependently inhibited the hydrolytic activity of Notum, showing the IC_{50} values of 18.73 ± 2.08, 76.67 ± 5.03, and 107.6 ± 10.44 nmol/L, 9.45 ± 1.38 and 12.84 ± 2.44 μmol/L, respectively (Fig. 4G−I, Fig. S28D and S28E). These findings suggested that three furanocoumarins (including 5-methoxypsoralen, psoralen, and isopsoralen) in BGZ acted as potent Notum inhibitors. Meanwhile, OPTS (a commonly used substrate for Notum) was used to verify the inhibitory effects of three newly identified potent Notum inhibitors that were discovered by **DO**-based fluorescence assay. As expected, 5-methoxypsoralen, isopsoralen, and psoralen could dose-dependently inhibit Notum-catalyzed OPTS hydrolysis, showing similar IC_{50} values of 11.21 ± 0.60, 71.86 ± 11.02, and 99.93 ± 10.85 nmol/L, respectively (Fig. 4J−L). These findings clearly demonstrate that the furanocoumarins, including 5-methoxypsoralen, isopsoralen, and psoralen, are potent anti-Notum constituents in BGZ, with IC_{50} values below 110 nmol/L.

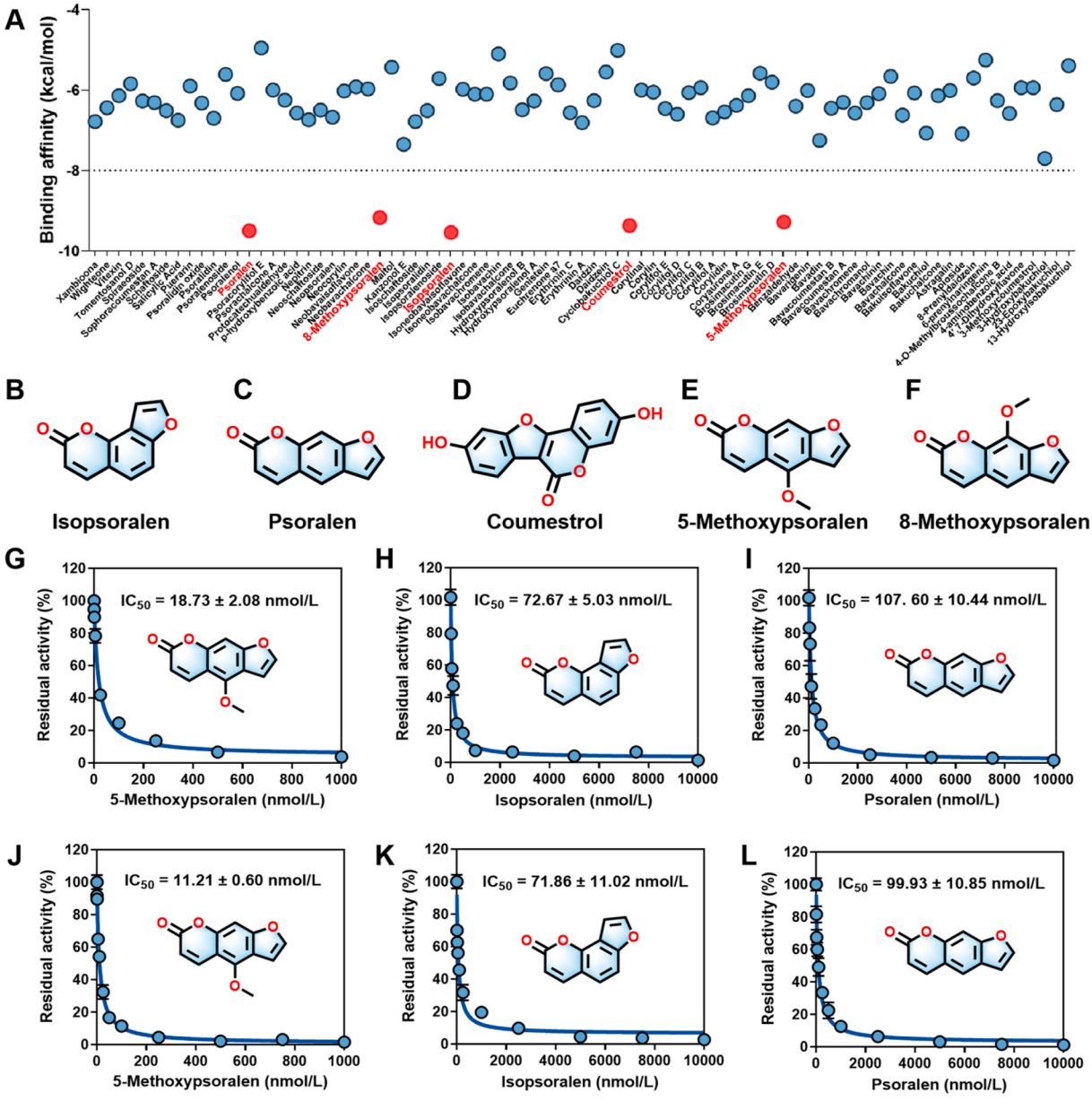

Figure 4 Discovering the key anti-Notum constituents in BGZ. (A) The predicted binding energies of all identified constituents in BGZ towards Notum. (B−F) The chemical structures for five constituents in BGZ with high binding affinities towards Notum. Dose-dependent inhibition curves of 5-methoxypsoralen (G), isopsoralen (H), and psoralen (I) against Notum-catalyzed **DO** hydrolysis. Dose-dependent inhibition curves of 5-methoxypsoralen (J), isopsoralen (K), and psoralen (L) against Notum-catalyzed OPTS hydrolysis. All data are expressed as mean ± SD ($n = 3$).

Table 1 Anti-Notum effects of 5-methoxypsoralen, isopsoralen, psoralen, 8-methoxypsoralen, and coumestrol.

Compound	Molecular formula	MW	Predicted binding energy (kcal/mol)	IC_{50} (DO as probe)
5-Methoxypsoralen	$C_{12}H_8O_4$	216.19	−9.27	18.73 ± 2.08 nmol/L
Isopsoralen	$C_{11}H_6O_3$	186.16	−9.62	72.67 ± 5.03 nmol/L
Psoralen	$C_{11}H_6O_3$	186.16	−9.58	107.60 ± 10.44 nmol/L
8-Methoxypsoralen	$C_{12}H_8O_4$	216.19	−9.19	9.45 ± 1.38 μmol/L
Coumestrol	$C_{15}H_8O_5$	268.22	−9.49	12.84 ± 2.44 μmol/L

3.5. Safety assessment of 5-MP, psoralen, and isopsoralen

Considering that anti-osteoporosis agents are typically required for long-term use, and some furanocoumarins have been reported with hepatotoxicity[48], it is necessary to investigate the safety profiles of three furanocoumarins with strong anti-Notum effects. In this work, the safety profiles of 5-methoxypsoralen (5-MP), isopsoralen, and psoralen were tested at a consecutive high dose of 200 mg/kg in mice (Fig. 5A). As shown in Fig. 5B, oral administration of 5-MP for 14 consecutive days in healthy mice showed favorable safety profiles, the overall mortality rate of 5-MP was 0% and no organ injury was observed. Serum biochemical indicator testing (Fig. 5C) demonstrated that oral administration of 5-MP decreased the levels of TC and TG in mice, but no significant difference in the serological indicators of organ injury (such as ALT, AST, CK, and CREA) was observed between 5-MP treated mice and the control group. Additionally, no significant difference in organ coefficient was observed, except a slight decline in the spleen coefficient (Fig. 5D). Pathological examination showed no observable organ injuries in the hearts, livers, spleens, lungs, or kidneys of mice following 5-MP treatment (Fig. 5E).

In sharp contrast, both isopsoralen and psoralen showed significant toxicity to healthy mice. As shown in Supporting Information Fig. S29A and S29B, after seven days of treatment with isopsoralen, the mice began to die, while their body weights significantly decreased. After oral administration of psoralen for 14 consecutive days, no death was observed in this group, but the body weights of psoralen-treated mice were decreased significantly. Compared to the control group, significant abnormalities in serum biochemical indicator levels were observed in mice plasma after oral administration of either psoralen or isopsoralen (Fig. S29C−S29J). Both psoralen and isopsoralen caused elevated serum levels of AST and ALT, suggesting that both agents could trigger liver damage. Moreover, psoralen could also elevate the levels of ALP, CREA, UREA, and TG in serum, while isopsoralen was found to decrease the levels of CK, UREA, and TG. As shown in Fig. S29K−S29M, the organ coefficients of the heart, liver, and kidney were remarkably elevated in both psoralen and isopsoralen-treated mice. Furthermore, H&E staining showed that both psoralen and isopsoralen resulted in varying degrees of organ injury (Supporting Information Fig. S30). Psoralen caused disrupted arrangement of cardiomyocytes and inflammatory infiltration, loosening of cell−cell junctions in the vicinity of liver lobules, and enlargement of cell gaps, accompanied by inflammatory infiltration in glomeruli. Similarly, isopsoralen induced inflammatory infiltration, disrupted the arrangement of cardiomyocytes, and increased necrotic cells and glomerular area in the liver. These observations clearly demonstrate that 5-MP displays favorable safety profiles, while psoralen and isopsoralen can cause multiple organ injuries in mice.

3.6. Inhibitory mechanisms of 5-MP against Notum

Next, the inhibitory mechanisms of 5-MP (the most potent Notum inhibitors identified from BGZ) against Notum were investigated by performing a suite of inhibition kinetic assays, computational simulations, as well as enzyme mutation and functional assays. As shown in Fig. 6A, 5-MP potently inhibited Notum-catalyzed **DO** hydrolysis in a competitive inhibition manner, showing a K_i value of 23.54 nmol/L. To validate the competitive inhibition manner of 5-MP against Notum, another Notum substrate OPTS (a commonly used substrate for Notum) was also used to verify the inhibitory mechanism of 5-MP against Notum. As expected, inhibition kinetic analyses showed that 5-MP strongly inhibited Notum-catalyzed OPTS hydrolysis in a competitive manner, with a K_i value of 15.10 nmol/L (Supporting Information Fig. S31). As shown in Fig. 6B and C, 5-MP could be well-docked into the catalytic cavity of Notum, where this agent formed strong $\pi-\pi$ stacking interactions and hydrogen bonding interactions with several surrounding amino acids (such as Trp128 and Phe268). These observations suggest that 5-MP acts as a canonical competitive inhibitor for Notum, while Trp128 and Phe268 may play important roles in Notum inhibition by 5-MP.

To further verify the crucial roles of Trp128 and Phe268 in the binding of 5-MP within the catalytic cavity of Notum, two mutates (including W128G, and F268G) of Notum were constructed. Functional assays revealed that the Notum mutate (W128G) totally lost the hydrolytic function after replacing Trp128 with Gly128, while the hydrolytic rate of **DO** in F268G Notum was also significantly decreased (Fig. 6D). These findings clearly suggested that both Trp128 and Phe268 in Notum played crucial roles in substrate recognition and catalysis. Docking simulations revealed that the distance between the carbonyl carbon of **DO** and the catalytic residue of the native Notum (Ser-232) was 4.0 Å, suggesting that **DO** could be easily hydrolyzed by native Notum (Fig. 6E). By contrast, W128G Notum showed that the distance between the ester bond of **DO** and the catalytic serine (Ser-232) was 7.0 Å (greater than 5 Å), making **DO** was hardly hydrolyzed by W128G Notum (Fig. 6F). To the best of our knowledge, this is the first report to reveal the crucial role of Trp128 in the enzymatic function of Notum.

We also tested the inhibitory potential of 5-MP against **DO** hydrolysis in F268G Notum. As shown in Supporting Information Fig. S32A, compared to the native Notum, the inhibitory effect of 5-MP against F268G Notum was significantly reduced (> 67-fold), showing the IC_{50} value of 1.21 μmol/L. Consistently, docking results showed that the binding affinity of 5-MP and F268G Notum was significantly weakened (−8.0 kcal/mol) compared to the native Notum (−9.27 kcal/mol) (Fig. S32B and Supporting Information Table S5). Meanwhile, the key amino acids involved in the interactions between 5-MP and F268G

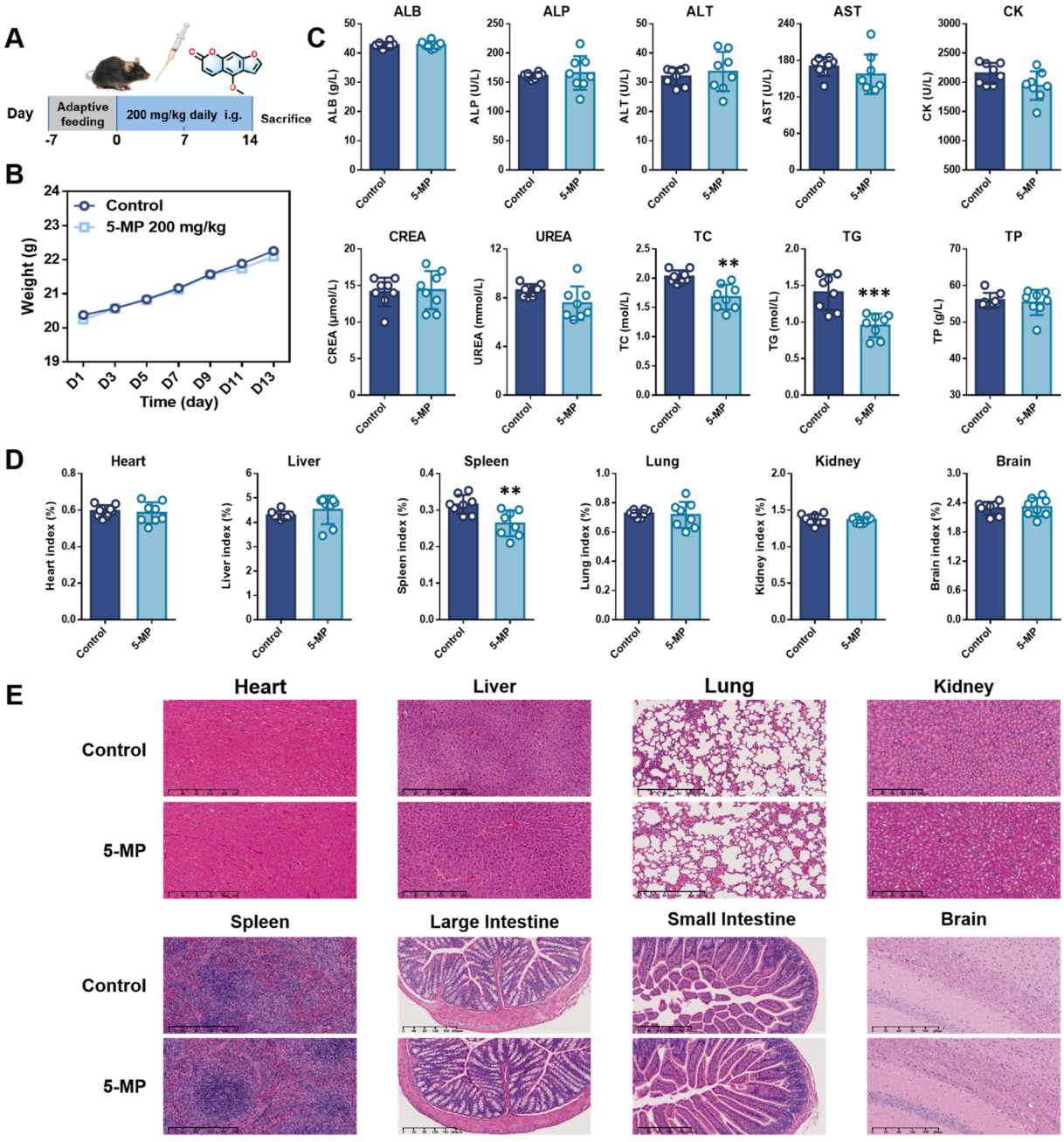

Figure 5 The safety profiles of 5-MP in healthy mice. (A) Animal experimental road map. (B) The changes in the body weight of mice. (C) The serum biochemical indicators in control mice and 5-MP-treated mice. (D) The organ coefficient ratios of control mice and 5-MP-treated mice. (E) H&E staining of heart, liver, spleen, lung, kidney, brain, large intestine, and small intestine in control and 5-MP groups. Scale bar = 200 μm. $^{**}P < 0.01$ *versus* Control, $^{***}P < 0.001$ *versus* Control. All data are expressed as mean ± SD ($n = 8$).

Notum were also changed compared to the native Notum (Fig. S32C and S32D). These findings suggest that both Trp128 and Phe268 of Notum profoundly affect the ligand recognition and substrate catalysis, while 5-MP could potently inhibit Notum *via* creating strong interactions with these two residues within the catalytic cavity of Notum.

3.7. *5-MP prompts osteoblast differentiation in MC3T3-E1 cells*

Previous studies have demonstrated that blocking Notum can promote osteoblast differentiation, restore normal trabecular bone structure, and increase cortical bone thickness and strength[23,25]. Considering that increased expression level of alkaline phosphatase (ALP) is an early indicator of osteoblast differentiation[49], the effects of 5-MP on ALP levels in MC3T3-E1 cells are first tested. As shown in Supporting Information Fig. S33A, dexamethasone (DXMS) could dose-dependently induce MC3T3-E1 cell injury, while approximately 50% of cells were diminished at 200 μmol/L. As shown in Fig. S33B−S33D, 5-MP, psoralen, and isopsoralen exhibited weak cytotoxicity towards MC3T3-E1 cells within the tested concentration range (0−20 μmol/L). Subsequently, the effects of 5-MP on the osteogenic differentiation of MC3T3-E1 cells

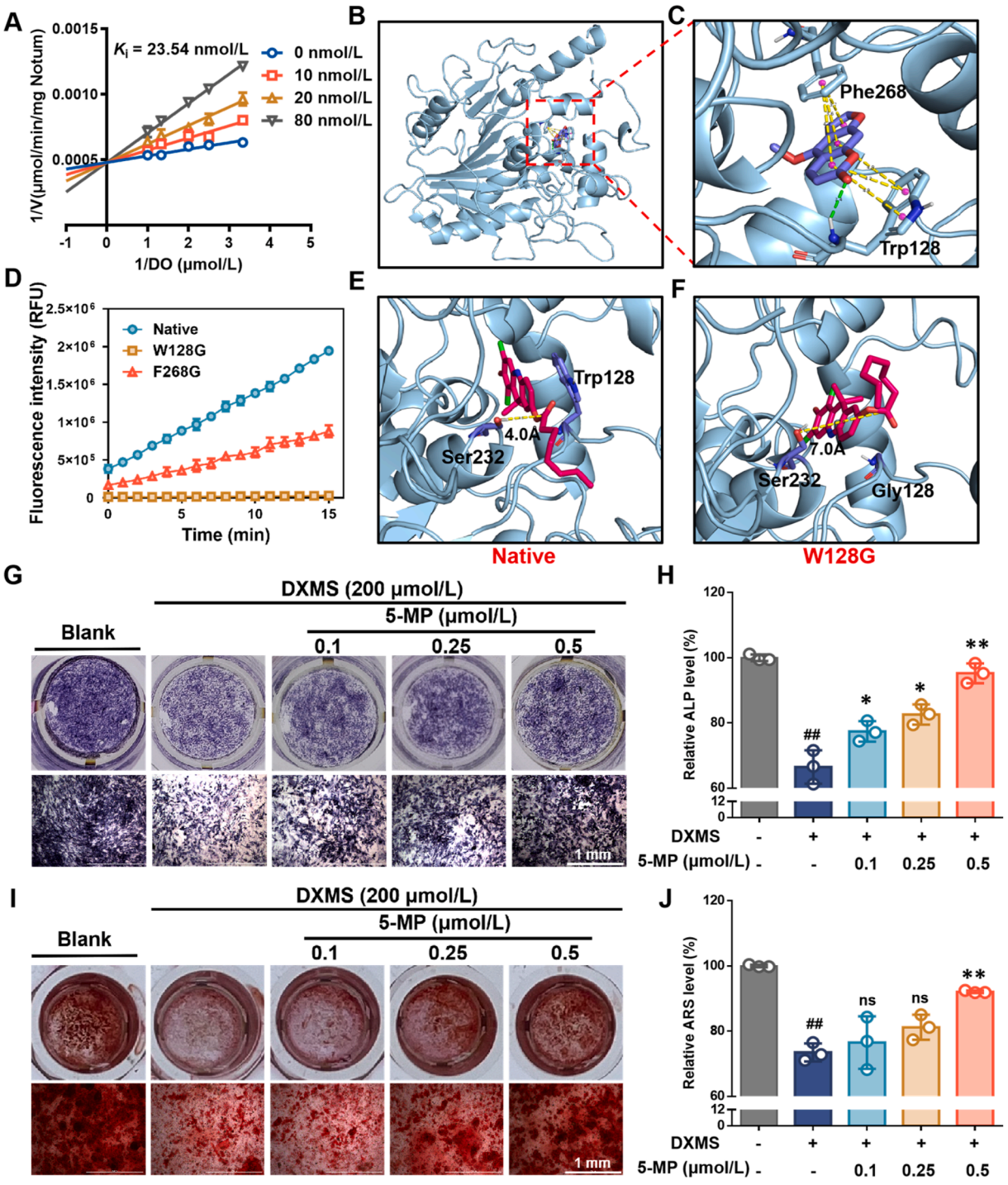

Figure 6 Inhibitory mechanisms of 5-MP against Notum. (A) Inhibition kinetics of 5-MP against Notum-catalyzed **DO** hydrolysis. (B) The stereo overview of molecular docking of 5-MP into the crystal structure of Notum (PDB ID: 7BLS). (C)The detailed view of 5-MP with Notum. (D) The hydrolytic rates of **DO** in native, W128G, and F268G Notum. (E) The detailed view of molecular docking of **DO** with native Notum. (F) The detailed view of molecular docking of **DO** with W128G Notum. (G) The effects of 5-MP on ALP levels in MC3T3-E1 cells under DXMS treatment. (H) The quantitative results correspond to Fig. 6G. (I) The imaging features of ARS staining of 5-MP. (J) The quantitative results corresponding to Fig. 6I. Scale bar = 1 mm. $^{\#}P < 0.05$ *versus* Blank; $^{\#\#}P < 0.01$ *versus* Blank; $^{\#\#\#}P < 0.001$ *versus* Blank; $^{ns}P > 0.05$ *versus* DXMS; $^{*}P < 0.05$ *versus* DXMS; $^{**}P < 0.01$ *versus* DXMS; $^{***}P < 0.001$ *versus* DXMS. All data are expressed as mean ± SD ($n = 3$).

were investigated. As shown in Fig. 6G and H, compared to the control cells (DMSO only), DXMS reduced the ALP level in MC3T3-E1 cells. As expected, 5-MP could dose-dependently mitigate the reduced ALP levels induced by DXMS, suggesting that 5-MP could significantly promote osteoblast differentiation *via* inhibiting Notum. Isopsoralen and psoralen could also exhibit osteoblast differentiation effects, but their promoting effects on osteoblast differentiation were relatively weak (Supporting

Information Fig. S34). Specifically, 5-MP at a low dose (0.5 μmol/L) showed more significant pro-differentiation effects on MC3T3-E1 cells than isopsoralen or psoralen at a relatively high dose (5 μmol/L).

The level of calcium salt is another key marker of bone cell proliferation and differentiation[50]. ARS forms complexes with calcium salts in a chelating manner, which is frequently used to assess intracellular calcification[51]. Herein, the promoting effects of 5-MP on osteogenic differentiation were verified by ARS staining. As shown in Fig. 6I and J, DXMS significantly inhibited calcification in MC3T3-E1 cells, while 5-MP significantly reversed the intracellular calcium loss triggered by DXMS. These results clearly suggest that 5-MP shows significant pro-differentiation effects on osteoblasts, which encourages us to further investigate the *in vivo* anti-osteoporosis effects of this phytochemical.

3.8. 5-Methoxypsoralen activates Wnt/β-catenin signaling in MC3T3-E1 cells

To validate whether 5-MP activates the Wnt/β-catenin signaling pathway in MC3T3-E1 cells by inhibiting Notum, the expression levels of Notum and several canonical indicators (including β-catenin, RUNX2 and GSK3β) of both Wnt signaling and osteoblast differentiation are examined following 5-MP treatment. As shown in Fig. 7A and B, compared to the control cells, DXMS significantly upregulated the mRNA levels of both Notum and GSK3β, as well as revised the mRNA levels of β-catenin, OPN and RUNX2 (Fig. 7C−E), suggesting that both Wnt signaling and osteoblast differentiation were suppressed. As expected, 5-MP significantly reversed the abnormal mRNA levels of these key indicators (Notum, GSK3β, β-catenin, OPN and RUNX2) induced by DXMS. Meanwhile, the protein levels of six key proteins (active β-catenin, β-catenin, OPN, RUNX2, Notum and GSK3β) related to Wnt signaling and osteoblast differentiation were also assayed. Similarly, compared to the control group, DXMS significantly up-regulated the protein levels of both Notum and GSK3β and down-regulated the protein levels of active β-catenin, total β-catenin, OPN and RUNX2. By contrast, 5-MP significantly reversed the abnormal protein expression of both Notum and GSK3β, as well as the reduced protein levels of active β-catenin, total β-catenin, OPN and RUNX2 that were triggered by DXMS (Fig. 7F−L). These findings suggest that 5-MP significantly activates the Wnt/β-catenin signaling pathway in osteoblasts and reverses DXMS-induced abnormal overexpression of both Notum and GSK3β, encouraging us to further investigate the anti-osteoporosis effects of 5-MP *in vivo*.

3.9. 5-MP shows favorable tissue distribution after intragastrical administration

Given the high structural similarity of both human Notum and mouse Notum (∼90%), mice are used for further pharmacological investigations (Supporting Information Table S6). Prior to the animal experiments, the tissue distribution of 5-MP in mice was carefully investigated to determine whether this agent could be distributed to bone tissue after intragastrical administration. As shown in Supporting Information Fig. S35, following a single oral dosing (40 mg/kg) of 5-MP in mice, 5-MP showed high exposure in the plasma and the liver. 5-MP was also detected in various tissues and organs of mice, especially in skeletal muscle and femur. Notably, the exposure levels of 5-MP in mice plasma (44.6 nmol/L, after administration 3 h) were much higher than the half-maximal inhibitory concentration of 5-MP against Notum (IC_{50} = 18.73 nmol/L), while the exposure level (8.3 nmol/L, after administration 2 h) of 5-MP in femur was comparable to its IC_{50} value. These findings clearly suggest that 5-MP can be well-absorbed into the circulating system and then distributed to the key organs for treating osteoporosis (such as the femur and skeletal muscle) after oral administration, indicating that this agent may be effective for treating osteoporosis *in vivo*.

3.10. 5-MP ameliorates DXMS-induced osteoporosis in mice

Encouraged by the above-mentioned findings, we next investigated the *in vivo* anti-osteoporosis effects of 5-MP in GIOP mice. As shown in Fig. 8A−C, DXMS could cause a significant reduction in body weight gain compared to the control group. Although neither PTH (positive control for osteoporosis) nor 5-MP (20 and 40 mg/kg) could significantly reverse the weight loss induced by DXMS, both PTH, and 5-MP remarkably improved the serum levels of four osteogenic markers, including alkaline phosphatase (ALP), osteocalcin/beta-glucuronidase (OT/BGT), osteoprotegerin (OPG), and Col-1A1. Compared to the control group, the serum levels of four markers were significantly decreased in DXMS-challenged mice, while both PTH and 5-MP (20 and 40 mg/kg) substantially increased the serum levels of all tested osteogenic markers (Fig. 8D−G).

Micro-CT imaging revealed sparse trabeculae and thinner cortical bone in DXMS-challenged mice compared to the control group (Fig. 9), confirming the successful establishment of the osteoporosis model. In contrast, 5-MP significantly improved both trabecular and cortical bone thickness. Micro-CT quantification revealed significantly greater trabecular and cortical bone thickness at both distal and mid-femur regions in 5-methoxypsoralen-treated mice compared to DXMS-challenged mice (Fig. 9B−E). 5-MP treatment significantly enhanced both bone volume fraction (bone volume fraction over total volume (BV/TV)) and bone mineral density (BMD) in distal and mid-femur regions (Fig. 9F−I). These micro-CT findings were corroborated by H&E staining (Fig. 10A). Most notably, double labeling demonstrated active new bone formation in 5-MP-treated mice, in stark contrast to the DXMS-challenged group (Fig. 10B).

Immunofluorescence analysis was also used to explore the spatial expression patterns of Notum in murine bone tissue. As shown in Fig. 10C, Notum (red) in the bone collected from healthy mice showed a very weak fluorescence signal, suggesting very low Notum expression levels in healthy mice. Compared to the healthy mice, the red signal of Notum was significantly increased in both cortical and cancellous bone tissues from DXMS-challenged mice, indicating that DXMS could upregulate Notum expression in both cortical and cancellous bone tissues. By contrast, either PTH or 5-MP significantly decreased the immunofluorescence signals of Notum in cortical bone tissues, but both agents hardly decrease the immunofluorescence signals of Notum in marrow cavity (Fig. 10C). Furthermore, the expression levels of Notum in mouse femurs were detected by Western blot analysis (Supporting Information Fig. S36). These findings suggested that both PTH and 5-MP effectively reverse Notum overexpression in cortical bone tissues of DXMS-challenged mice. These observations clearly show that 5-MP is an efficacious anti-GIOP agent, capable of significantly mitigating DXMS-induced osteoporosis in mice

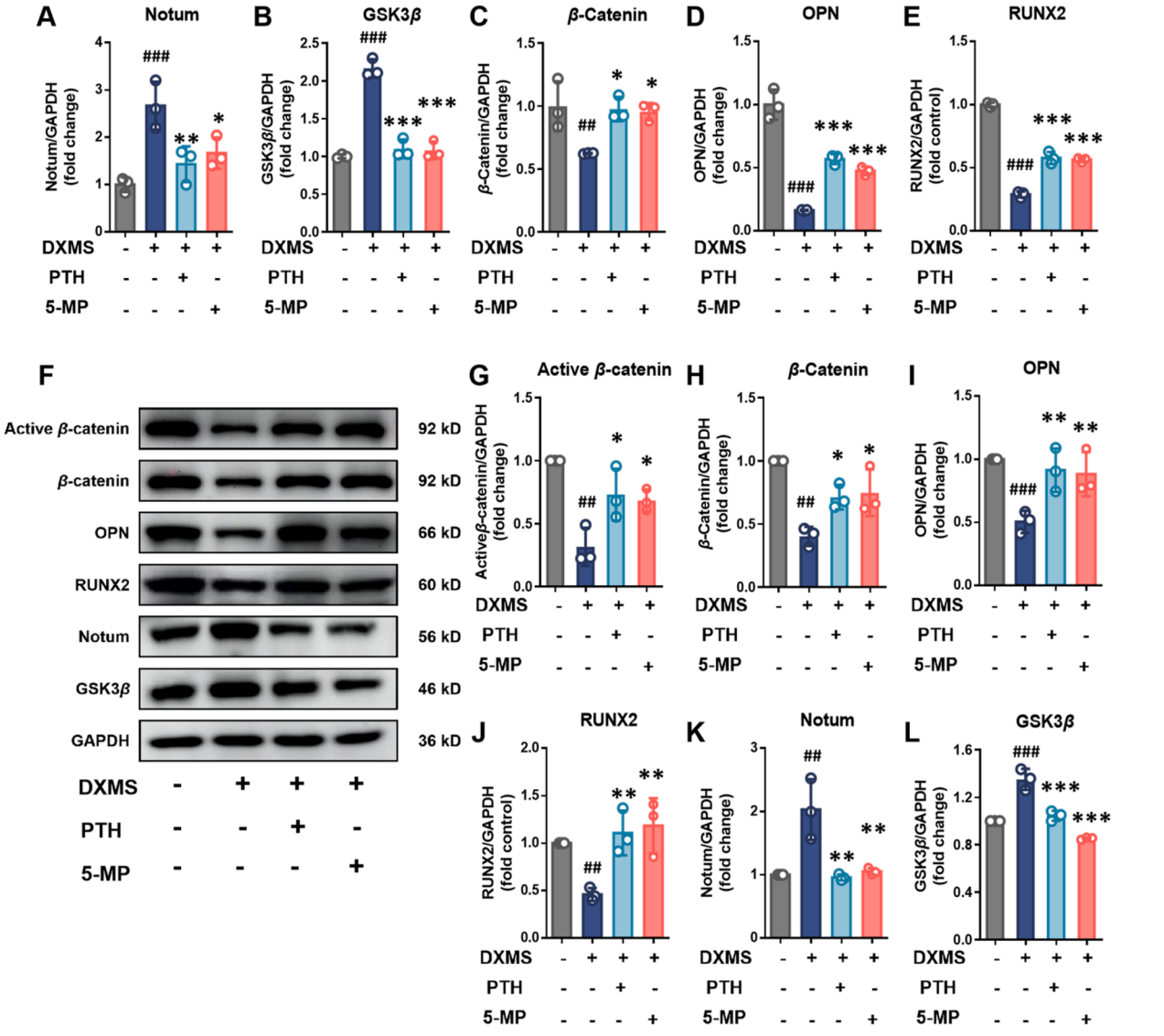

Figure 7 The newly identified anti-Notum agent 5-MP activates Wnt/β-catenin signaling in MC3T3-E1 cells. Relative mRNA levels of Notum (A), GSK3β (B), β-catenin (C), OPN (D) and RUNX2 (E) in DXMS-challenged MC3T3-E1 cells with or without PTH and 5-MP treatment. (F) The regulatory effects of PTH and 5-MP on the protein levels of activeβ-catenin, β-catenin, OPN, RUNX2, Notum, and GSK3β in MC3T3-E1 cells. Statistical analysis of protein expression (G−L). Data are represented as mean ± SD from three independent assays. $n = 3$. $^{\#}P < 0.05$ *versus* Control; $^{\#\#}P < 0.01$ *versus* Control; $^{\#\#\#}P < 0.001$ *versus* Control, $^{*}P < 0.05$ *versus* DXMS; $^{**}P < 0.01$ *versus* DXMS; $^{***}P < 0.001$ *versus* DXMS.

via inhibiting the hydrolytic activity of Notum and reversing DXMS-induced Notum overexpression.

4. Discussion

Notum, a palmitoyl protein carboxylase, has attracted increasing attention due to its crucial role in blocking the Wnt signaling[20]. Growing evidence suggests that Notum is a druggable regulator of the Wnt signaling, and has been validated as a promising therapeutic target for treating GIOP. Studies have demonstrated that the knockdown of Notum or pharmacological inhibiting Notum activity would bring markedly positive effects on enhancing both bone density and cortical bone thickness in mice[25]. However, to the best of our knowledge, the potent Notum inhibitors with favorable safety profiles are rarely reported. Inspired by the clinical efficacy of some commonly used herbal medicines (HMs) for treating GIOP, we aimed to identify the potent Notum inhibitors from HMs. To directly assess the anti-Notum activities of HMs, we have devised a rapid-responding and high binding-affinity NIR fluorescent substrate for Notum (termed **DO**), which emits a long emission wavelength (660 nm) and shows a high signal-noise ratio. Phytochemicals in HMs, such as coumarins and flavonoids, are known to emit fluorescence signals, but their emission wavelengths are typically short (< 560 nm). Thus, the **DO**-based biochemical assay minimizes interference from the background fluorescence emitted by phytochemicals in crude HM extract (Supporting Information Table S7).

With **DO** in hand, we subsequently constructed a practical platform for high-throughput screening and characterization of HMs with anti-Notum effects. The anti-Notum effects of more than

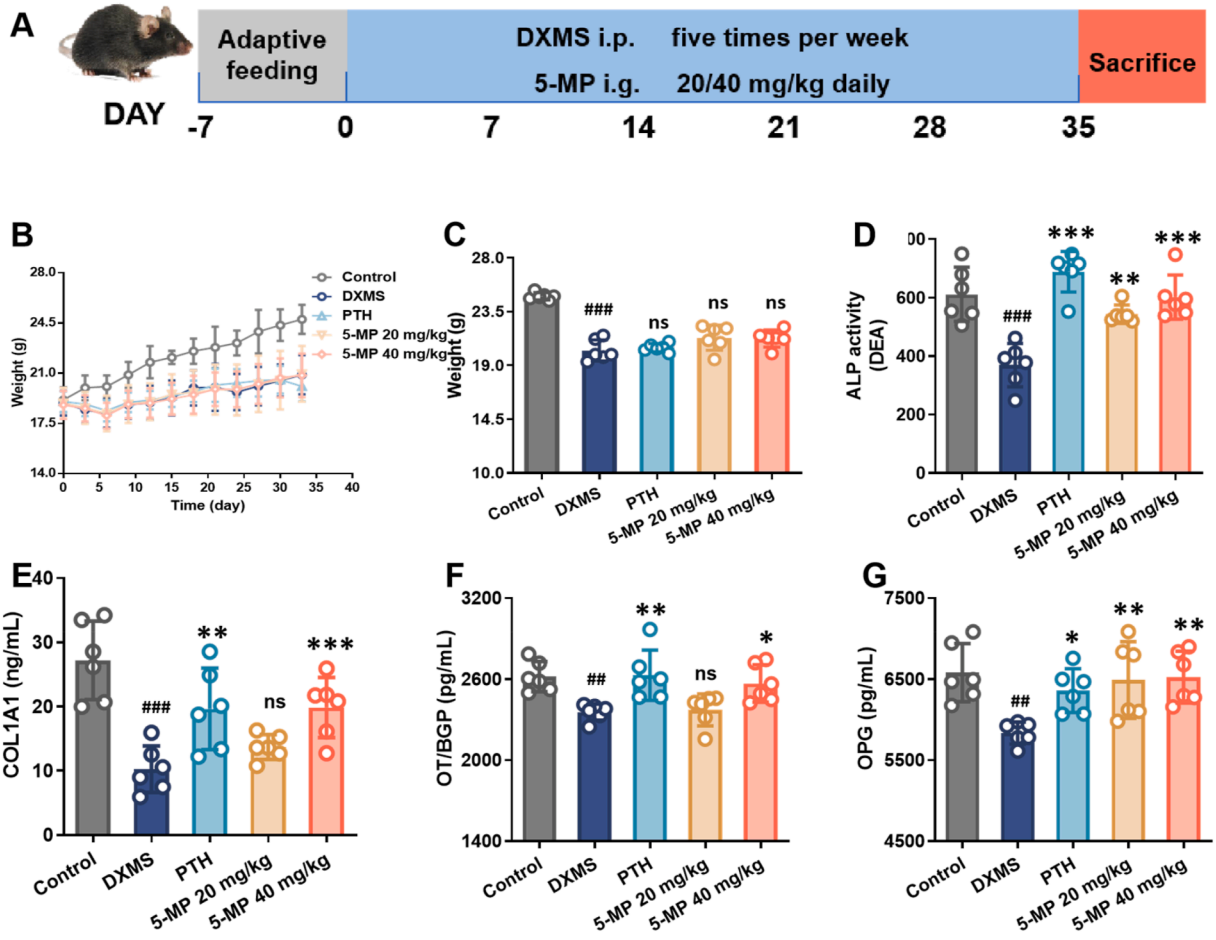

Figure 8 The therapeutic effects of 5-MP against DXMS-induced osteoporosis in mice. (A) The detailed schedule of animal experiments. Body weight of the mice during the experiment (B), and the comparison of the body weights within each experimental group at the last weighing(C). The bone metabolism index of serum levels, including ALP (D), COL1A1 (E), OT/BGP (F), and OPG (G). $^{\#\#}P < 0.01$ *versus* Control; $^{\#\#\#}P < 0.001$ *versus* Control, $^{ns}P > 0.05$ *versus* DXMS, $^{*}P < 0.05$ *versus* DXMS; $^{**}P < 0.01$ *versus* DXMS; $^{***}P < 0.001$ *versus* DXMS. All data are expressed as mean ± SD ($n = 6$).

100 HMs were screened using **DO** as the fluorogenic substrate. Interestingly, our results showed that BGZ, a commonly used anti-osteoporosis drug in clinical settings, potently inhibited Notum-catalyzed **DO** hydrolysis (IC_{50} = 6.98 μg/mL). Given that Notum only has a single ligand-binding cavity and all reported naturally occurring inhibitors of Notum are competitive inhibitors, we adopted an efficient strategy for discovering Notum inhibitors by integrating docking-based virtual screening and **DO**-based biochemical assay. The results revealed that five selected constituents (including isopsoralen, psoralen, coumestrol, 5-methoxypsoralen, and 8-methoxypsoralen) with high binding affinities (predicted binding energy < −9.0 kcal/mol) all exhibited anti-Notum activity, with three of these compounds showed potent anti-Notum effects (IC_{50} < 110 nmol/L). Notably, all of these newly identified Notum inhibitors in BGZ are furanocoumarins, suggesting that the furanocoumarins are the key anti-Notum constituents in BGZ. Meanwhile, these agents could also serve as lead compounds for developing more efficacious Notum inhibitors. These results clearly demonstrate the utility of docking-based screening of Notum inhibitors for the efficient discovery of Notum inhibitors, which guides the rapid discovery of Notum inhibitors from HMs.

Among the newly identified three furanocoumarins with strong anti-Notum effects, 5-methoxypsoralen showed the best combination of both pharmacological activity and safety. In contrast, both isopsoralen and psoralen showed evident organ injuries, suggesting that these agents could not be suitable for long-term administration for treating GIOP. These findings also suggested that introducing a methoxy moiety at the C-5 site of furanocoumarin could strongly enhance anti-Notum activity while improving safety *in vivo*. Increasing evidence indicates that compounds containing furan rings may be metabolically activated by mammalian cytochrome P450 enzymes (CYPs) to generate reactive intermediates, which further covalently bind to GSH or macromolecules to trigger hepatotoxicity. By contrast, hepatotoxicity was significantly reduced when the furan ring was saturated. *In vitro* assays found that both psoralen and isopsoralen could be metabolically bioactivated by CYPs to generate reactive intermediates, which further covalently bind to GSH. However, 5-methoxypsoralen was preferentially metabolized by CYP enzymes to produce a stable metabolite (5-hydroxypsoralen), which could be further metabolized by phase II metabolizing enzymes (such as UDP-glucuronosyltransferase enzymes) and

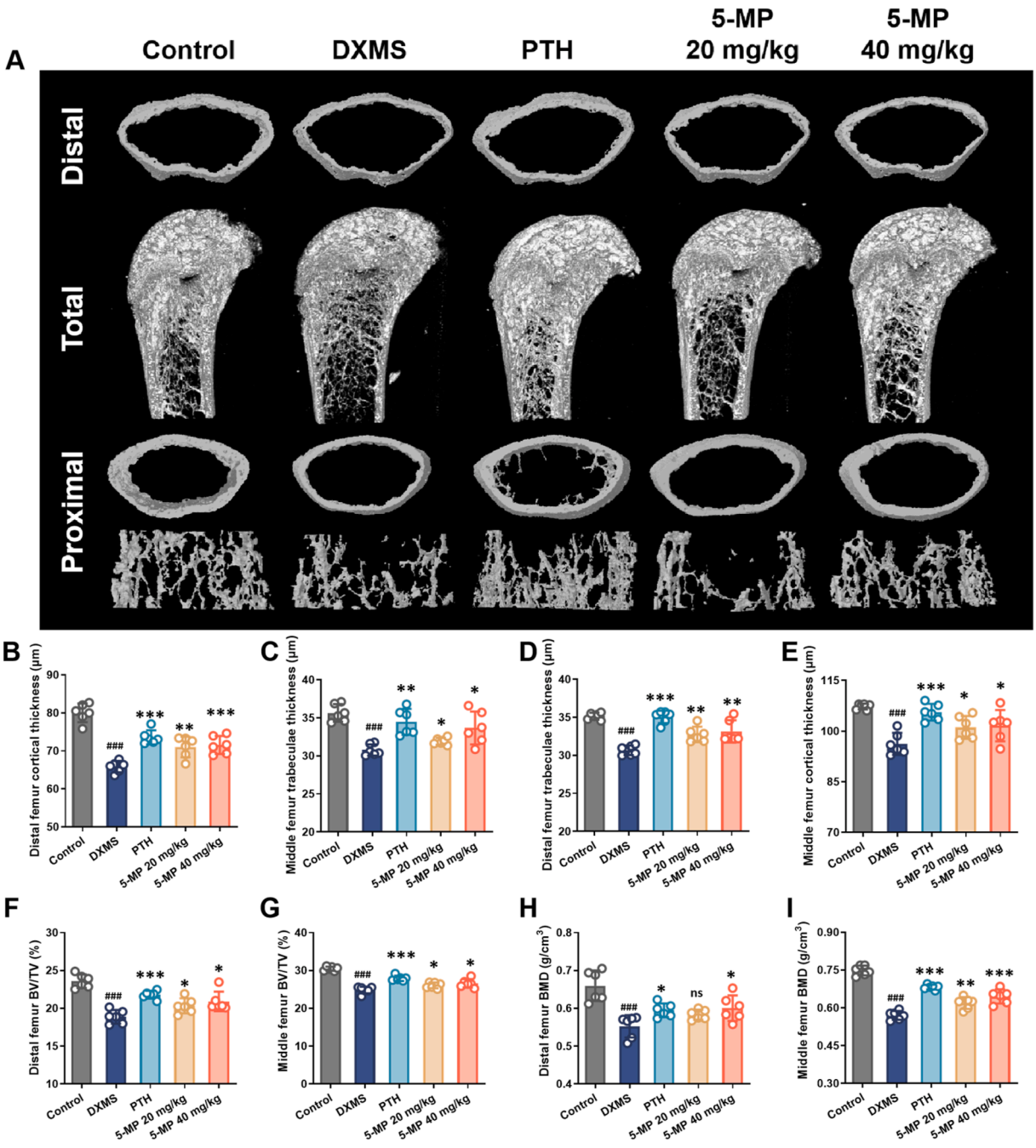

Figure 9 The therapeutic effects of 5-MP against DXMS-induced pathological osteoporosis. (A) The characteristic images of micro-CT illustrate the distal femur bone and trabecular bone. The contrastive analyses of the cortical thicknesses (B), trabecular thicknesses (C), BV/TV (%) (D), and BMD (E) of the distal femur. The contrastive analyses of the cortical thicknesses (F), trabecular thicknesses (G), BV/TV (%) (H), and BMD (I) of the middle femur. $^{\#\#\#}P < 0.001$ *versus* Control, $^{*}P < 0.05$ *versus* DXMS; $^{**}P < 0.01$ *versus* DXMS; $^{***}P < 0.001$ *versus* DXMS. All data are expressed as mean ± SD ($n = 6$).

then excreted from the body. Meanwhile, we did not detect reactive intermediates of 5-MP in phase I metabolic systems using GSH as a trapping agent. These findings partially explain why 5-methoxypsoralen shows high safety profiles in mice without any observations of hepatotoxicity. In the future, medicinal chemists can design more furanocoumarin derivatives as potent Notum inhibitors by saturating the furan ring or introducing additional metabolically labile sites for CYPs.

Notably, most of the reported Notum inhibitors show relatively weak anti-Notum effects (Supporting Information Table S8), while most of them have not been subjected to *in vivo* tests, such as safety assessment, and *in vivo* anti-GIOP effects. By contrast, 5-MP, a naturally occurring Notum inhibitor, demonstrates significant anti-osteoporosis activity at both the cellular and animal levels, as well as showing favorable safety profiles *in vivo*. Given its favorable safety profile, high oral bioavailability (69.6%−

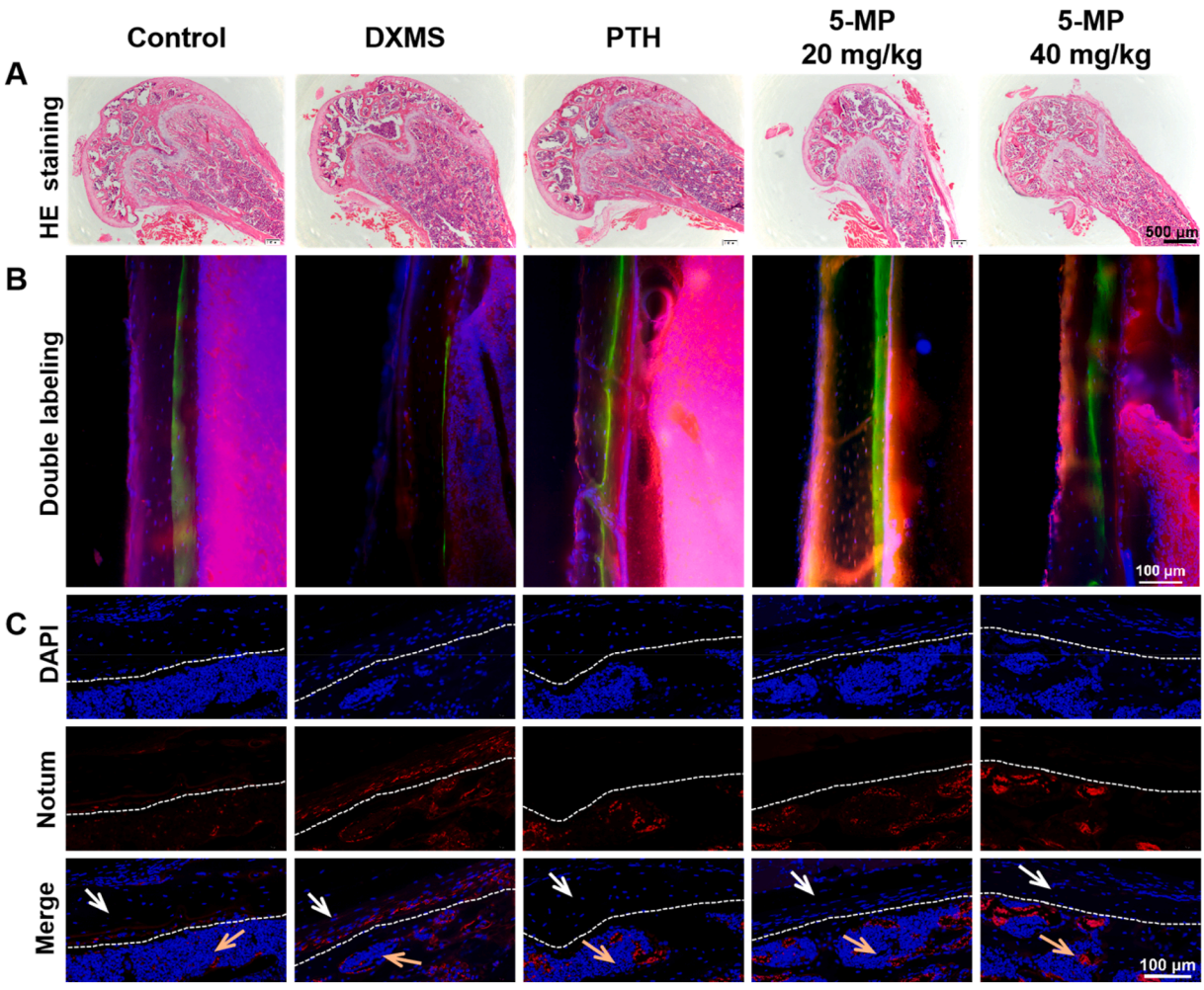

Figure 10 5-MP ameliorates DXMS-induced osteoporosis in mice. (A) H&E staining of the distal femur bone. Scale bar: 500 μm. (B) The characteristic images of double labeling. Scale bar: 100 μm. (C) Immunofluorescence imaging of distal femur bone, blue for DAPI, and red for Notum. Scale bar: 100 μm. The white arrows indicate cortical bone, and the orange arrows indicate marrow. The white lines indicate the location of the cortical bone above and the marrow cavity below.

94.0% in rats)[52,53] and relatively long half-life ($t_{1/2}$ = 4.21 h)[54], long-term oral administration of 5-methoxypsoralen may result in higher plasma exposure levels and enhanced anti-osteoporosis effects. In this work, we quantified the exposure levels of 5-methoxypsoralen in plasma and the femur after a single oral dose of 5-methoxypsoralen (40 mg/kg) to mice. The results showed that the plasma exposure levels of 5-methoxypsoralen (44.6 nmol/L) were much higher than the half-maximal inhibitory concentration of 5-methoxypsoralen against Notum (IC_{50} = 18.73 nmol/L), while the exposure level (8.3 nmol/L) of 5-methoxypsoralen in the femur was comparable to its half-maximal inhibitory concentration. Notum is an exocytosis protein, and 5-methoxypsoralen in the circulating system can bind to the peripheral Notum secreted by osteoblasts. These findings provide an explanation for why 5-MP could significantly alleviate DXMS-induced osteoporosis and activate Wnt/β-catenin signaling in mice, suggesting that 5-MP may serve as a promising lead compound for developing novel anti-GIOP agents. In the future, structural modifications on 5-MP or bone-targeted drug delivery systems of 5-MP should be performed to get more efficacious anti-Notum agents or to elevate the bone-targeting ability of this agent. Furthermore, it has been reported that activating Wnt/β-catenin signaling is a feasible strategy for liver regeneration[55-57]. Considering that Notum is highly expressed in the liver, and the newly identified Notum inhibitor (5-MP) prefers to be distributed into the liver, 5-MP can be used as a potent activator of Wnt/β-catenin signaling to promote liver regeneration. In the future, the *in vivo* efficacy of 5-MP for promoting liver regeneration should be investigated systematically.

5. Conclusions

In summary, this work showcases a practical and efficient platform for discovering naturally occurring potent Notum inhibitors from HMs for combating GIOP. Firstly, **DO**, a rapid-responding near-infrared fluorogenic substrate for Notum was developed to construct a practical fluorescence-based high-throughput screening assay, which was then used for assessing the anti-Notum potentials of the commonly used HMs. Following high-throughput screening, BGZ, a frequently used anti-osteoporosis herb, was found with strong and competitive inhibition on Notum. After that, a highly efficient strategy was

adopted to uncover the key anti-Notum constituents in BGZ, *via* integrating phytochemical profiling, docking simulation-based virtual screening, and **DO**-based biochemical assays. The results demonstrate that three furanocoumarins in BGZ, including 5-MP, psoralen, and isopsoralen, are naturally occurring potent Notum inhibitors (IC_{50} < 110 nmol/L). Among these three furanocoumarins, 5-MP showed favorable safety profiles and impressive anti-osteoporosis effects. 5-MP could strongly promote calcium formation and activate Wnt signaling in DXMS-challenged MC3T3-E1 osteoblasts. A tissue distribution study showed that 5-MP could distribute into bone and skeletal muscle following oral administration in mice. Subsequent *in vivo* tests showed that 5-MP markedly enhanced bone density and increased the thickness of cancellous and cortical bone in DXMS-induced osteoporotic mice. Collectively, a practical and integrated strategy was constructed for efficiently identifying the key anti-Notum constituents from herbal medicines, while 5-MP, a newly identified Notum inhibitor from the Chinese herb BGZ, holds great promise for treating GIOP and promoting bone repair.

Acknowledgments

This study was supported by the National Natural Science Foundation of China (82273897, U23A20516, 82104281, and 32101202), Organizational Key Research and Development Program of Shanghai University of Traditional Chinese Medicine (2023YZZ02, China), Shanghai Municipal Health Commission's TCM research project (2022CX005, China), Innovation Team and Talents Cultivation Program of National Administration of Traditional Chinese Medicine (ZYYCXTDD-202004, China), Three-year Action Plan for Shanghai TCM Development and Inheritance Program (ZY(2021−2023)-0401, China), the Fundamental Research Funds for the Central Universities (G2024KY05106, China), and the State Key Laboratory of Fine Chemicals, Dalian University of Technology (KF2202, China), and supported by China Postdoctoral Science Foundation (2024M762108, China). The authors thank Dr. Yuguang Zhao from University of Oxford (UK) for providing very helpful suggestions.

Author contributions

Guangbo Ge and Yuqing Song designed this work. Yuqing Song, Feng Zhang, and Jia Guo carried out the experiments and performed data analysis. Zhenhao Tian contributed to the design and chemical synthesis of substrates. Yufan Fan, Hairong Zeng, Mengru Sun, Jun Qian, Shenglan Qi, and Zihan Chen participated in part of the experiments. Yunqing Song, Baoqing Yu, analyzed the data and provided advice on the interpretation of the data. Yuqing Song and Feng Zhang wrote the manuscript. Guangbo Ge, Jia Guo, Xudong Jin, Zhi Qian, Tian Tian, and Yao Sun revised the manuscript. All of the authors have read and approved the final manuscript.

Conflicts of interest

The authors declare that there are no conflicts of interest.

Supporting information

Supporting information to this article can be found online at https://doi.org/10.1016/j.apsb.2025.06.004.

References

1. Compston JE, McClung MR, Leslie WD. Osteoporosis. *Lancet* 2019;**393**:364−76.
2. Ensrud KE, Crandall CJ. Osteoporosis. *Ann Intern Med* 2024;**177**:Itc1−16.
3. de Villiers TJ. Bone health and menopause: osteoporosis prevention and treatment. *Best Pract Res Clin Endocrinol Metabol* 2024;**38**:101782.
4. Aibar Almazán A, Voltes Martínez A, Castellote Caballero Y, Afanador Restrepo DF, Carcelén Fraile MDC, López Ruiz E. Current status of the diagnosis and management of osteoporosis. *Int J Mol Sci* 2022;**23**:9465.
5. Sözen T, Özışık L, Başaran N. An overview and management of osteoporosis. *Eur J Rheumatol* 2017;**4**:46−56.
6. Peng CH, Lin WY, Yeh KT, Chen IH, Wu WT, Lin MD. The molecular etiology and treatment of glucocorticoid-induced osteoporosis. *Cí-Jì Yixué* 2021;**33**:212−23.
7. Liang H, Zhao J, Tian T. Pharmacological interventions for glucocorticoid-induced osteoporosis: an umbrella review. *Horm Metab Res* 2023;**55**:511−9.
8. Madamsetty VS, Mohammadinejad R, Uzieliene I, Nabavi N, Dehshahri A, Garcia Couce J, et al. Dexamethasone: insights into pharmacological aspects, therapeutic mechanisms, and delivery systems. *ACS Biomater Sci Eng* 2022;**8**:1763−90.
9. Humphrey MB, Russell L, Danila MI, Fink HA, Guyatt G, Cannon M, et al. 2022 American college of rheumatology guideline for the prevention and treatment of glucocorticoid-induced osteoporosis. *Arthritis Rheumatol* 2023;**75**:2088−102.
10. MacDonald BT, Tamai K, He X. Wnt/β-catenin signaling: components, mechanisms, and diseases. *Dev Cell* 2009;**17**:9−26.
11. Gao Y, Chen N, Fu Z, Zhang Q. Progress of Wnt signaling pathway in osteoporosis. *Biomolecules* 2023;**13**:483.
12. Marini F, Giusti F, Palmini G, Brandi ML. Role of Wnt signaling and sclerostin in bone and as therapeutic targets in skeletal disorders. *Osteoporos Int* 2023;**34**:213−38.
13. Wang T, Liu X, He C. Glucocorticoid-induced autophagy and apoptosis in bone. *Apoptosis* 2020;**25**:157−68.
14. Sheridan C. Wnt is back in drugmakers' sights, but is it druggable? *Nat Biotechnol* 2018;**36**:1028−9.
15. Zhao Y, Schuhmacher LN, Roberts M, Kakugawa S, Bineva-Todd G, Howell S, et al. Notum deacylates octanoylated ghrelin. *Mol Metabol* 2021;**49**:101201.
16. Baetta R, Banfi C. Dkk (Dickkopf) proteins. *Arterioscler Thromb Vasc Biol* 2019;**39**:1330−42.
17. Huang J, Ma T, Wang C, Wang Z, Wang X, Hua B, et al. SOST/-Sclerostin impairs the osteogenesis and angiogesis in glucocorticoid-associated osteonecrosis of femoral head. *Mol Med* 2024;**30**:167.
18. Claudel M, Jouzeau JY, Cailotto F. Secreted Frizzled-related proteins (sFRPs) in osteo-articular diseases: much more than simple antagonists of Wnt signaling? *FEBS J* 2019;**286**:4832−51.
19. Nusse R, Clevers H. Wnt/β-catenin signaling, disease, and emerging therapeutic modalities. *Cell* 2017;**169**:985−99.
20. Bayle ED, Svensson F, Atkinson BN, Steadman D, Willis NJ, Woodward HL, et al. Carboxylesterase Notum is a druggable target to modulate Wnt signaling. *J Med Chem* 2021;**64**:4289−311.
21. Kakugawa S, Langton PF, Zebisch M, Howell S, Chang TH, Liu Y, et al. Notum deacylates Wnt proteins to suppress signalling activity. *Nature* 2015;**519**:187−92.
22. Li C, Yang P, Liu B, Bu J, Liu H, Guo J, et al. Prednisolone induces osteocytes apoptosis by promoting Notum expression and inhibiting PI3K/AKT/GSK3β/β-catenin pathway. *J Mol Histol* 2021;**52**:1081−95.
23. Movérare Skrtic S, Nilsson KH, Henning P, Funck Brentano T, Nethander M, Rivadeneira F, et al. Osteoblast-derived Notum reduces cortical bone mass in mice and the Notum locus is associated with bone mineral density in humans. *FASEB J* 2019;**33**:11163−79.

24. Choi RB, Bullock WA, Hoggatt AM, Horan DJ, Pemberton EZ, Hong JM, et al. Notum deletion from late-stage skeletal cells increases cortical bone formation and potentiates skeletal effects of sclerostin inhibition. *J Bone Miner Res* 2021;**36**:2413−25.
25. Brommage R, Liu J, Vogel P, Mseeh F, Thompson AY, Potter DG, et al. Notum inhibition increases endocortical bone formation and bone strength. *Bone Res* 2019;**7**:2.
26. Zhang L, Li X, Ying T, Wang T, Fu F. The use of herbal medicines for the prevention of glucocorticoid-induced osteoporosis. *Front Endocrinol* 2021;**12**:744647.
27. Feng Z, Chuncheng W, Bing W, Shipeng X. Effects of *Psoraleae fructus* extract bone metabolism levels in ovariectomized rats with osteoporosis. *J Ethnopharmacol* 2024;**16**:35−8.
28. Kim M, Kim H-S, Oh J, Zhou X, Ahn S, Koo Y, et al. Ameliorative effects of Kyung-Ok-Ko and its mixture with *Pueraria lobata* Ohwi on postmenopausal osteoporosis by promoting phytoestrogenic activity in rats. *Front Nutr* 2023;**10**:1171346.
29. Zhao Y, Svensson F, Steadman D, Frew S, Monaghan A, Bictash M, et al. Structural insights into notum covalent inhibition. *J Med Chem* 2021;**64**:11354−63.
30. Mahy W, Patel M, Steadman D, Woodward HL, Atkinson BN, Svensson F, et al. Screening of a custom-designed acid fragment library identifies 1-phenylpyrroles and 1-phenylpyrrolidines as inhibitors of notum carboxylesterase activity. *J Med Chem* 2020;**63**:9464−83.
31. Zhao Y, Jolly S, Benvegnu S, Jones EY, Fish PV. Small-molecule inhibitors of carboxylesterase Notum. *Future Med Chem* 2021;**13**:1001−15.
32. Zhao Y, Ren J, Hillier J, Jones M, Lu W, Jones EY. Structural characterization of melatonin as an inhibitor of the Wnt deacylase Notum. *J Pineal Res* 2020;**68**:e12630.
33. Zhao Y, Ren J, Hillier J, Lu W, Jones EY. Caffeine inhibits Notum activity by binding at the catalytic pocket. *Commun Biol* 2020;**3**:555.
34. Atkinson BN, Steadman D, Mahy W, Zhao Y, Sipthorp J, Bayle ED, et al. Scaffold-hopping identifies furano[2,3-*d*]pyrimidine amides as potent Notum inhibitors. *Bioorg Med Chem Lett* 2020;**30**:126751.
35. Atkinson BN, Steadman D, Zhao Y, Sipthorp J, Vecchia L, Ruza RR, et al. Discovery of 2-phenoxyacetamides as inhibitors of the Wnt-depalmitoleating enzyme NOTUM from an X-ray fragment screen. *MedChemComm* 2019;**10**:1361−9.
36. Mahy W, Willis NJ, Zhao Y, Woodward HL, Svensson F, Sipthorp J, et al. 5-Phenyl-1,3,4-oxadiazol-2(3*H*)-ones are potent inhibitors of Notum carboxylesterase activity identified by the optimization of a crystallographic fragment screening hit. *J Med Chem* 2020;**63**:12942−56.
37. Song L, Sun M, Shi J, Tian Z, Song Y, Liu H, et al. Rational construction of a novel bioluminescent substrate for sensing the tumor-associated hydrolase Notum. *Anal Chem* 2023;**95**:5489−93.
38. Sun MR, Song LL, Wei HZ, Shi JH, Zhao B, Tian T, et al. Rational construction of a practical enzyme-activatable fluorogenic substrate for hNotum and its applications in functional imaging and inhibitor screening. *Sens Actuators B Chem* 2023;**393**:134145.
39. Song L, Sun M, Song Y, Zhang F, Zhao B, Zeng H, et al. Rationally engineered IR-783 octanoate as an enzyme-activatable fluorogenic tool for functional imaging of hNotum in living systems. *Chin Chem Lett* 2024;**35**:109601.
40. Yang Y, Xiong Y, Zhu G, Sun M, Zou K, Zhao Y, et al. Discovery of seven-membered ring berberine analogues as highly potent and specific hCES2A inhibitors. *Chem Biol Interact* 2023;**378**:110501.
41. Li W, Zhang Y, Wu Y, Zhu G, Liu X, Song Y, et al. New bysspectin A derivatives as potent inhibitors of human carboxylesterase 2A. *Eur J Med Chem* 2023;**259**:115708.
42. Shi JH, Zhao B, Song LL, Song YQ, Sun MR, Tian T, et al. Chalcone derivatives as novel, potent and selective inhibitors against human Notum: structure−activity relationships and biological evaluations. *Chin Chem Lett* 2024;**35**:108405.
43. Ominsky MS, Vlasseros F, Jolette J, Smith SY, Stouch B, Doellgast G, et al. Two doses of sclerostin antibody in cynomolgus monkeys increases bone formation, bone mineral density, and bone strength. *J Bone Miner Res* 2010;**25**:948−59.
44. Qian J, Li Q, Song Y, Gong X, Hu K, Ge G, et al. Pectolinarigenin ameliorates osteoporosis *via* enhancing Wnt signaling cascade in PPARβ-dependent manner. *Phytomedicine (Stuttg)* 2024;**129**:155587.
45. Hu WD, Wang SY, Xu AC, Wang XY, Gao XM, Yang WZ. Characterization and identification of chemical components in traditional Chinese medicine *Psoraleae fructus* based on UHPLC−Q-TOF−MS. *China J Chin Mater Med* 2023;**48**:2989−99.
46. Zhang X, Zhao W, Wang Y, Lu J, Chen X. The chemical constituents and bioactivities of *Psoralea corylifolia* Linn: a review. *Am J Chin Med* 2016;**44**:35−60.
47. Ting H, Yinjie W, Yingying Z, Ting M, Lijuan Y, Sen Y. Chemical composition analysis of *Psoraleae fructus* alcohol extract by UPLC−Q-TOF−MS and its mechanisms of promoting melanogenesis. *Nat Prod Res Dev* 2024;**36**:968−981+53.
48. Li W, Lin D, Gao H, Xu Y, Meng D, Smith CV, et al. Metabolic activation of furan moiety makes diosbulbin B hepatotoxic. *Arch Toxikol* 2016;**90**:863−72.
49. Vimalraj S. Alkaline phosphatase: structure, expression and its function in bone mineralization. *Gene (Amst)* 2020;**754**:144855.
50. Zhu S, Chen W, Masson A, Li YP. Cell signaling and transcriptional regulation of osteoblast lineage commitment, differentiation, bone formation, and homeostasis. *Cell discovery* 2024;**10**:71.
51. Huang C, Wang Y. Downregulation of METTL14 improves postmenopausal osteoporosis *via* IGF2BP1 dependent posttranscriptional silencing of SMAD1. *Cell* 2022;**13**:919.
52. Yu XA, Azietaku JT, Li J, An M, He J, Hao J, et al. The pharmacokinetics, bioavailability and excretion of bergapten after oral and intravenous administration in rats using high performance liquid chromatography with fluorescence detection. *Chem Cent J* 2016;**10**:62.
53. Liang Y, Xie L, Liu K, Cao Y, Dai X, Wang X, et al. Bergapten: a review of its pharmacology, pharmacokinetics, and toxicity. *Phytother Res* 2021;**35**:6131−47.
54. Liao M, Song G, Cheng X, Diao X, Sun Y, Zhang L. Simultaneous determination of six coumarins in rat plasma and metabolites identification of bergapten *in vitro* and *in vivo*. *J Agric Food Chem* 2018;**66**:4602−13.
55. Zhao L, Jin Y, Donahue K, Tsui M, Fish M, Logan CY, et al. Tissue repair in the mouse liver following acute carbon tetrachloride depends on injury-induced Wnt/β-catenin signaling. *Hepatology (Baltim, Md)* 2019;**69**:2623−35.
56. Russell JO, Monga SP. Wnt/β-catenin signaling in liver development, homeostasis, and pathobiology. *Annu Rev Pathol* 2018;**13**:351−78.
57. Zou G, Park JI. Wnt signaling in liver regeneration, disease, and cancer. *Clin Mol Hepatol* 2023;**29**:33−50.